Universidade de Aveiro Departamento de Engenharia Mecânica
2009

Mauro André
Oliveira Simões

Desenvolvimento de um Robô Aéreo para Inspecção e Monitorização

Development of an Aerial Robot for Inspection and Surveillance

Mauro André
Oliveira Simões

Desenvolvimento de um Robô Aéreo para Inspecção e Monitorização

Dissertação apresentada à Universidade de Aveiro para cumprimento dos requisitos necessários à obtenção do grau de Mestre em Engenharia Mecânica, realizada sob a orientação científica de Prof. Dr. Vítor Manuel Ferreira dos Santos, Departamento de Engenharia Mecânica, Universidade de Aveiro.

o júri / the jury

presidente / president	**Prof. Doutor Robertt Angelo Fontes Valente** Professor Auxiliar do Departamento de Engenharia Mecânica
arguente / examiner	**Prof. Doutor Carlos Batista Cardeira** Professor Auxiliar do Departamento de Engenharia Mecânica do Instituto Superior Técnico
orientador / adviser	**Prof. Doutor Vítor Manuel Ferreira dos Santos** Professor Associado do Departamento de Engenharia Mecânica

agradecimentos / acknowledgements

Ao completar mais uma fase do meu percurso académico, é com o maior orgulho que aqui presto os meus sinceros agradecimentos às pessoas que contribuíram para a realização desta dissertação, a qual não seria possível sem o seu apoio e ajuda.

Ao Professor Doutor Vítor Santos pela sua orientação, disponibilidade, espírito crítico e ideias que tão importantes foram no êxito deste projecto.

Gostaria de agradecer aos colegas do Laboratório de Automação e Robótica pelo excelente ambiente de trabalho proporcionado, mas mais concretamente ao Eduardo Durana e ao Hugo Tavares, pela pronta disponibilidade na resolução de qualquer problema.

Ao meus amigos André e Eduardo quero-lhes agradecer pela ajuda que me deram na elaboração e correcção da tese. Ao Rodrigo pelo tempo, paciência e ajuda indespensável na construção do protótipo do robô. Um agradecimento especial à Aldara pela compreensão, apoio e carinho que tanto me ajudaram nesta fase da minha vida.

Este projecto contou com a colaboração do departamento de Química, que numa fase inicial nos disponibilizaram o hélio necessário para este projecto. Quero agradecer à Cláudia Simões, Cristina Barros e ao presidente do conselho directivo, Fernando Amado, pela atenção e simpatia que sempre demonstraram.

Finalmente, um muito obrigado os meus pais, por me terem proporcionado e incentivado ao longo do meu percurso académico, que sem o vosso esforço e dedicação não seria possível.

Palavras-chave Robótica aérea, UAV, UAS, telemetria, Interface gráfica, algoritmos de controlo.

Resumo

Os veículos aéreos não tripulados são cada vez mais procurados para desempenhar diversas tarefas do quotidiano. Estes sistemas são, no entanto, caros e necessitam de equipas grandes para serem operados.

O controlo de veículos aéreos autónomos num ambiente parcialmente conhecido é uma tarefa complexa. Os sistemas actuais são baseados em sensores e sistemas de controlo relativamente dispendiosos, e são frequentemente pesados, necessitando de uma grande quantidade de energia.

O principal objectivo deste projecto é desenvolver um sistema aéreo não tripulado, fácil de operar, para inspecção e monitorização. Integrados neste sistema encontram-se a plataforma do robô aéreo, o sistema de controlo e a estação de controlo remoto.

A plataforma desenvolvida é baseada em veículos mais leves que o ar. Pretende-se que esta plataforma seja capaz de navegar por espaços confinados e também em ambientes fechados. A esta plataforma foram incorporados sensores e sistemas de controlo leves e de baixo consumo de energia.

Para a estação de supervisão foi desenvolvido um programa que permite o controlo do robô e supervisão dos objectivos da missão. A interface gráfica permite de uma forma intuitiva efectuar o controlo do robô.

Os testes iniciais permitiram demonstrar as capacidades dos sistemas desenvolvidos para atingir os objectivos propostos.

Keywords Aerial Robotics, UAV, UAS, telemetry, graphical interface, control algorithms.

Abstract

Unmanned aerial vehicles are being increasingly sought to perform every days tasks. But these systems are still costly and require a large crew of mission controllers and pilots to adequately manoeuvre the UAV.

Managing and control an autonomous air vehicle in a partially known and uncontrolled environment is a complex problem. Current UAVs are based on costly sensors and control systems. These control systems are also usually heavy and demand large amounts of power.

This thesis aims to develop an easy to operate unmanned aerial system for surveillance and monitoring missions. As part of this system will be developed an aerial platform, the embedded control system, the ground station with a graphical interface.

The platform designed is based on a small lighter-than-air vehicle. To successfully complete the mission objectives the UAV must be capable of navigate through constrained areas and endow indoor flights. The UAV is equipped with low power consumption sensors and processors.

For the ground station will be developed an application to control and monitor the UAV status. The graphical user interface application provide an easy to use interface to control and monitor the mission objectives.

The initial tests allowed to validate the feasibility of the systems developed to achieve the proposed goals.

Contents

List of Figures

List of Tables

Acronyms

ADC	Analog-to-Digital Converter
AEW	Airborne Early Warning
API	Application Programming Interface
CG	Center of Gravity
COTS	Commercial-Off-The-Shelf
CPU	Central Processing Unit
DIY	Do It Yourself
DOF	Degrees-Of-Freedom
DOP	Dilution Of Precision
DSP	Digital Signal Processing
FOS	Factor Of Safety
GPS	Global Positioning System
GUI	Graphical User Interface
HILS	Hardware In Loop Simulation
I^2C	Inter-Integrated Circuit
IC	Integrated Circuit
IMU	Inertial Measurement Unit
INS	Inertial Navigation Systems
I/O	Input/Output
ISR	Intelligence, Surveillance and Reconnaissance
LAR	*Laboratório de Automação e Robótica*
LED	Light-Emitting Diode
LTA	Lighter-Than-Air
MAV	Micro Aerial Vehicles
MCU	MicroController Unit
MEMS	MicroElectricalMechanical Systems
MIPS	Million Instructions Per Second
MR	MagnetoResistive
NMEA	National Marine Electronics Association
PCB	Printed Circuit Board
PWM	Pulse-Width Modulation
RC	Radio Controlled
RF	Radio-Frequency
SMT	Surface-Mount Technology
TTL	Transistor–Transistor Logic
UART	Universal Asynchronous Receiver/Transmitter
UAS	Unmanned Aerial System
UAV	Unmanned Aerial Vehicle
UGV	Unmanned Ground Vehicle
UTC	Universal Time, Coordinated
VTOL	Vertical Take-Off and Landing
WAAS	Wide Area Augmentation System
WDT	WatchDog Timer

"I'm an idealist. I really think people can change the world ..."

– Chris Anderson, DIY drone co-founder

Chapter 1

Introduction

This chapter presents the motivation on the base of this thesis and defines the objectives for the project.

An introduction to unmanned aerial vehicles (UAVs), discussing their relevance over the history of aviation, is made. Then, a brief technical introduction to UAVs and to control techniques is made, describing different platform systems, highlighting their advantages, weakest points and the target missions of each platform.

On section 1.4 the organization of this thesis is presented.

1.1 Motivation

Unmanned aerial vehicles have demonstrated for long time its importance in military ISR missions; in particular, the conflicts in the Middle East, the Balkans and Afghanistan have demonstrated their flexibility to perform different military tasks. With the feedback provided, by military missions, a wide range of possible applications was found and UAVs have increasingly being implemented in civilian tasks. Moreover, in the next 10 years, industry analysts expect the acquisition market for UAS to exceed USD$44 billion in the U.S. market alone [46].

Still, less attention has been given to the possible civilian applications of these vehicles. However, there is a huge application potential for UAVs, as described in section 1.3.2, and the benefits of their implementation are clear.

Besides the large interest and development around aerial robots, their cost is still very high and prohibitive for civilian tasks, where the budget is limited and the benefit-to-cost ratio is a key factor. Constraining their applications to military missions and some research projects.

Current inspection and surveillance missions are preformed by rotatory-wing aircrafts and lighter-than-air vehicles. These solutions are based on costly sensors, which usually are not adequate for these tasks, and these platforms were rather bigger or provide too less flight endurance, such as helicopter-like platforms. The main parcel of the budget is spent with avionics and other electronic devices, needed to accomplish the task, and often reach US$10,000 to US$50,000 or more [5, 35].

This project is inserted in the LAR (Laboratório de Automação e Robótica), Mechanical Engineering Department, Aveiro University, where there is active research with the

unmanned ground vehicles (UGV), but until now no aerial vehicle was used as research platform. Moreover, this is the first project, that the author is aware, of an aerial robot in the University of Aveiro. Developing an aerial robot is one of the most complete tasks of engineering, embracing knowledge as diverse as aerodynamics, electronics, signal processing, solid mechanics, modeling and programming.

Thus, the main goal of this thesis is to develop an unmanned aerial system adapted to inspection and surveillance missions, but still holding enough flexibility to be used as platform for future research projects. This system is intended to be as robust, low-cost, reliable and easily adapted to other mission scenarios as possible.

1.2 Objectives

The main goals of this thesis are to develop an unmanned aerial vehicle, able of carry out inspection and surveillance tasks in indoor and outdoor environments. The robot is designed to be used as a low-cost platform for building inspection, and as a movable camera for open-air surveillance. Thus, the vehicle must endow a long endurance flight, be capable of manoeuvring in constrained areas and be robust enough to withstand outdoors weather conditions, up to some limits.

It is mandatory to carry sensors to estimate the robot position and attitude, while still leaving some space to add other sensors and actuators that can be useful for future projects. These sensors must be capable of providing a sufficient amount of information to the operator. In order to lead to a successful mission. The on-board control system is responsible for processing the sensors' information, and retrieve the robot pose to the ground station.

For this robot, an high level of autonomy is required. In order to make it more independent of continuous communications with the ground station and also leaving the operator more focused on the mission objectives. Endowing the robot with the ability to deal with many different types of situations, reduces the level of detailed control required by the operator, greatly increasing the system's value and effectiveness. It must also retain the ability, if the operator demands it, to be directly operated.

The robot will be remotely monitored by a graphical interface, where the missions' parameters can be inserted in real-time. The ground station will receive the telemetry data through a 2.4GHz data link to refresh the information displayed by the graphical interface.

This thesis does not aim primarily on advancing the UAV technologies nor improve a specific characteristic of those vehicles, but rather on the development of an new UAS as a whole. As part of the UAS we intend to develop an autonomous aerial platform, the electronic control system, and the ground station with the graphical user interface (GUI).

A secondary objective is to reduce the implementation time and costs of new robots. Therefore, there is the intention to design the control board independently from the platform, enabling its use in other UAV and UGV robots.

1.3 Unmanned Aerial Vehicles

Unmanned Aerial Vehicles have always been tied to the history of aviation. Since the firsts trials, and even before potential applications of unmanned aircraft have surfaced, engineers were convinced that there was a need to operate flying machines without the presence of humans on board [25]. Following the achievements of the Langley, and later on, by the Wright brothers, several successful scaled unmanned flight trials were carried out [36]. These tests aimed at gathering data on the forces acting during the flight, experimenting new designs and control philosophies, ultimately leading to the first, globally accepted, successful manned self-powered flight, in December 1903 by Wilbur Wright [36].

The first successful powered flight was unmanned, presumably to reduce the risk to the pilot and to allow a smaller and less expensive vehicle. These are the very same reasons which promote UAV technologies nowadays.

Samuel P. Langley of the Smithsonian Institution developed a steam-powered tandem-monoplane that first flew successfully over the Potomac river in May, 1986, being considered the first heavier-than-air craft [44]. Figure 1.1 depicts one of the steam-powered unmanned air planes built by Langley.

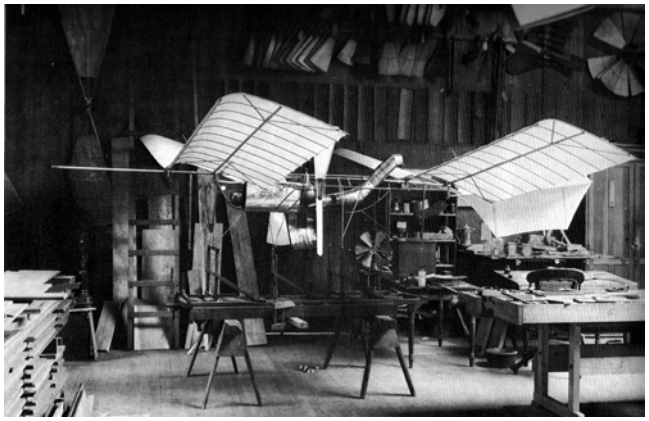

Figure 1.1: Photograph of Aerodrome No. 5, a steam powered UAV built by Samuel Langley in 1896.

At the start of World War I, heavier-than-air powered aircraft had become practical for reconnaissance, artillery spotting, and even attacks against ground positions [22]. Since the beginning of the first World War, the aviation has shown its importance on the battlefield, when its use in critical reconnaissance halted the initial German offensive against Paris [22].

Current applications of UAVs are very close to the ones of the airplanes in the early days of aviation. Some of the most relevant applications are: missions of reconnaissance and observation, search and rescue operations, forest fire surveillance and payload delivery.

Unmanned air vehicles are self-propelled air vehicles that are either remotely controlled or are capable of conducting autonomous missions [39]. There are numerous varieties of UAVs, and the term UAV itself can be associated with many types of machines. The first UAV built by Wright brothers was no more than a glider controlled by ropes; today, the

term UAV is commonly associated with aerial robots which have some level of autonomy. These aerial robots are equipped with sensors that can sense the surrounding environment and, sometimes, also interact with it.

The term Aerial Robotics can be associated with *robotic flying machines* (mission-independent, platform-oriented concept); however, it could also mean *robotics that use flying machines* (platform-independent, mission-oriented concept). Robotic flying machines are commonly referred to as unmanned aerial vehicles; while entire infrastructures, which include systems and human components required to operate such machines for a given operational objective, are often called unmanned aerial systems (UASs) [25] .

1.3.1 Common platforms

UAVs can vary greatly in form and shape, e.g., fixed-wing vehicles, helicopters, flapping wing systems and lighter-than-air (LTA) machines . Four different UAV designs can be seen in figure 1.2.

(a) The predator, a fixed-wind UAV from USAF.

(b) R-max helicopter.

(c) Mercury project developed by AeroEnvironment.

(d) Project DIVA, an lighter-than-air blimp [8].

Figure 1.2: Examples of different UAV configurations.

Each configuration has specific advantages, which makes each configuration more suited for some missions. Fixed-wing models, for its higher stamina and flight speeds, enables them to cover larger areas, and are best suited to reconnaissance and long range

combat missions. Helicopters offer a great manoeuvrability, and are suited to low altitude flight in urban areas. Flapping wing are usually classified as micro-UAV systems – for their tiny sizes – and can easily be disguised, therefore they are adequate to perform spy missions and can also be deployed inside buildings. Lighter-than-air aircrafts have flight characteristics compared to helicopters, but their higher stamina, lower cost and maintenance makes these vehicles more attractive as UAV platforms.

Each task has its own specifications, concerning the characteristics of the UAV, but almost all of them benefit from the ability to maintain a hovering condition, be able to take off in a limited space and from an augmented manoeuvrability, to operate in constrained areas. And, perhaps the most important, be capable of carrying a substantial payload, needed to transport electronic systems but also to accommodate cargo (missiles, chemicals, and other products). Vertical take-off and landing (VTOL) aerial robots have the best arrangement of all of these parameters.

The first aircrafts capable of doing systematic controlled flights were lighter-than-air non-rigid airships, but as the technology was getting more advanced, rigid airships began having some success. Rigid airships allowed larger aircrafts, and became the first aircrafts to transport passengers and cargo over great distances. Rigid-structure dirigibles were more capable than fixed-wing aircraft in terms of pure cargo carrying capacity, for decades.

From the early 1950s trough 1962, the United States of America Navy was already using this type of vehicles equipped with sensors to conduct patrol missions. US Navy worked with an 123 meter long airship, used as airborne early warning (AEW) system, this airship was equipped with radars for surveillance and was operated by a crew of 24 people [22].

Lighter-than-air aircrafts are also known as airships, dirigibles, or blimps when referring more specifically to non-rigid airships. A blimp does not have an internal structural framework – instead, the lifting gas is stored in an inflatable container called envelop. The increased pressure inside the envelop maintains the airbag in its shape.

Blimps are the most common type of airships. This particular type of LTA non-rigid vehicles have simpler structure and they can be easily transported when deflated. In figure 1.3 is demonstrated the blimp components and typical lighter-than-air platform configuration.

The envelop is made from a thin plastic film, and is were the helium is stored. In the gondola is kept the electronic components, like the control system power supply and to the gondola are also attached the main thrusters. The main thrusters enable the control of the vehicle over the 3-D plane, the tail thruster provide more effectiveness in turning manoeuvres. The rear stabilizers, in small blimps, are used for stability proposes only. But in larger airships they can also be used to control the vehicle when fitted with movable surfaces.

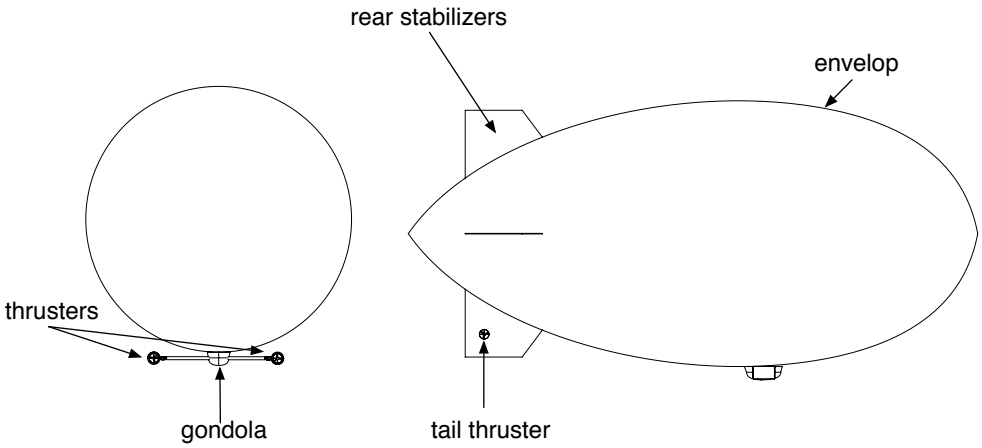

Figure 1.3: Blimp components identification.

When compared to other types of VTOLs, blimps are less noisy, provide more flight endurance and are inherently stable, but also have disadvantages such as slower speeds, and due to the amount of helium needed to provide lift they are frequently larger, difficult to deploy and with significant manoeuvrability constrains [39].

Since these types of vehicles are relatively slow, have larger sizes and higher inertial moments, they are very sensitive to wind gusts, which can make the implementation of this vehicles, for outdoor tasks, quite daunting.

A commercial radio-controlled blimp sold for advertising proposes can be seen in figure 1.4.

Figure 1.4: Radio Controlled advertisement blimp from GreenZeppelin at Forum Ciência Viva.

1.3.2 Current applications

Aerial Robots are used successfully to perform various tasks, mostly in the military intelligence, surveillance and reconnaissance (ISR) missions context, but they are being increasingly used for homeland security, civilian applications and as research platforms.

The advantages offered by UAVs are numerous and accrue most noticeably in certain mission areas [42]. The unique ability to perform long endurance missions, the capability to hover and their disposability are a great benefit over manned aircraft. Prime examples include flying close to a forest fire to look for stranded individuals, searching in contaminated areas, and identifying potential radioactive leaks after a nuclear reactor accident [42].

The main current applications of UAVs are classified in four groups [25]:

- Aerial Observations;
- Military Operations;
- Civilian and Private Applications;
- Payload delivery.

Some of the most important applications of these categories are: border patrol, infrastructure surveillance, inspection of man-made structures, archaeological site prospection, critical assets and environmental monitoring missions, shore surveillance and military recognition, advertising and traffic monitoring. The figure 1.5 depicts a Raven UAV being deployed in Iraq. Raven flew in various missions that aided in force protection, provided reconnaissance for patrols and surveilled the perimeter of camps.

Figure 1.5: Raven UAV in use by US army [5].

Unfortunately, as almost any technology breakthrough, UAVs have also been used by terrorists in their campaigns. On July 2006, the Hezbollah attacked an Israeli warship

and an Egyptian civilian vessel with missiles launched from UAVs [32]. As the analysis of technical capabilities shows, UAVs can become a very attractive option for terrorists anxious to deliver an attack with chemical or biological weapons [33].

Unmanned aerial vehicles can be flown quickly and systematically over an wide area to locate victims of an accident or a natural disaster, and then establish visual contact with objects at the site or stranded victims to guide rescue forces to the scene [42]. UAVs can also be more readily deployed in weather conditions that would normally prevent human piloted search and rescue, and can help focus the efforts of search and rescue crews to the rescue operation instead of the time consuming search operation.

UAVs have been the type of robots most used in real disasters or tested in these scenarios. Five Silver Fox, in figure 1.6, equipped with thermal imaging technology to detect the body heat of storm survivors, was used in New Orleans after the hurricane Katrina, in 2005. This was the first time that UAVs were used on an large-scale disaster [25]. The UAVs flew above flooded areas and provided real-time information directly to the rescue crews.

Figure 1.6: Silver Fox small tactical UAV [38].

After this first real implementation, the lessons learned were primarily related to how much, geographically distributed disasters influence the choice of robot modality, and how they can be used. These disasters highlighted the need for miniature aerial vehicles which could provide viewpoints of 1 to 10 kilometres [25].

1.3.3 Flight control and perception

Human interfaces are a critical point when talking about UAVs. Graphical User Interfaces (GUI), such as the one presented in figure 1.7, promote the interaction between the operator and the robot, empowering the user to monitor the robot states, and are crucial for the mission success. GUIs are usually primitive and need substantial training and attention from the user.

Some challenges that GUI face and have been target of research in this field are the *human-to-robot* ratio – currently a single robot requires from two to three humans, depending on configuration and mission; these operators need to be extensively trained, and GUIs do not provide sufficient situation awareness [25].

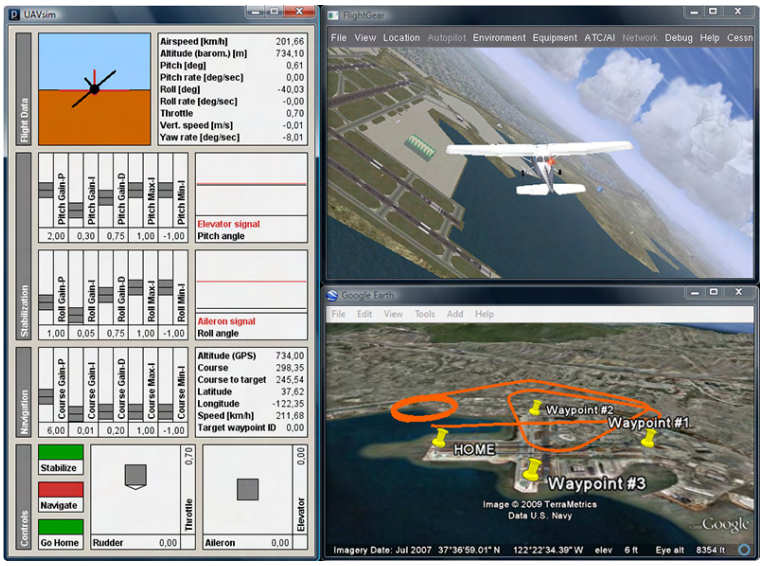

Figure 1.7: Uavplayground project, a GUI with GPS tracking waypoint and circling navigation [24].

The level of autonomy provided by a UAV will depend on the aircraft's autonomous decision capabilities. It can be influenced by the objective that the robot is designed for, and ranges from low-level flight control algorithm design - commonly known as augmented reality - to high level fully autonomous machines [39].

Various levels of autonomy are proposed and described below [42]:

- Tele-operation: the operator has full control;
- Tele-autonomy: the operator gives abstract-level commands and has access to pre-interpreted sensor data;
- Shared autonomy: the robot and the operator are seen as "on-pair" partners in performing a joint task;
- Full autonomy: the robot performs the task entirely by its own, without any human assistance.

Most current UAV systems are typically flown using remote control during all critical phases of the mission, while using on-board navigation systems to maintain flight path. These systems are remotely controlled by an operator or a crew of operators (one as a pilot, the others as payload specialists), by choosing way-points or by directly controlling the UAV.

Autonomous way-point navigation of fixed-wind platforms was available for rescue teams of hurricane Katrina but it was not used; instead, responders were much more interested in actively directing the UAVs [25]. This suggests that the ultimate control regime will not be one of full autonomy, but instead one which enables the controller to use the robot as if it were an extension of himself, enabling the crew of operators to have a better perception of the surroundings and the vehicle itself.

Robot tele-operation relies only on the pilot skills to successfully navigate the UAV; this demands permanent attention from the operator, causing fatigue in a short period of time and it might lead to poor performance and reduce safety of the robot. An unmanned helicopter flight close to a building, in inspection missions, usually do not last more than 10 minutes, due to pilot fatigue. Tele-operation is also inherently dependent on a good communication between the ground station and the robot, if it fails the robot is left without control and the consequences can be severe.

Tele-autonomy concept slightly reduces this problems; yet, communication failure or an inappropriate controller decision caused by excessive workload, can still compromise the mission and cause damage to the robot.

In shared autonomy design the robot is endowed with more autonomy, enabling the robot to perform tasks in an autonomous way. In this approach, also known as *mixed initiative* and *collaborative control* [42], the operator is able to interact with the robot modeling, deliberation to provide guidance and control. From the ground station the operator is able to introduce new way-points, modify the parameters for some decisions and tune the algorithm responsible for the blimp response. This cooperation is depicted by figure 1.8, where the higher-level modules (Modeling and Deliberation) are present in both the robot and control station.

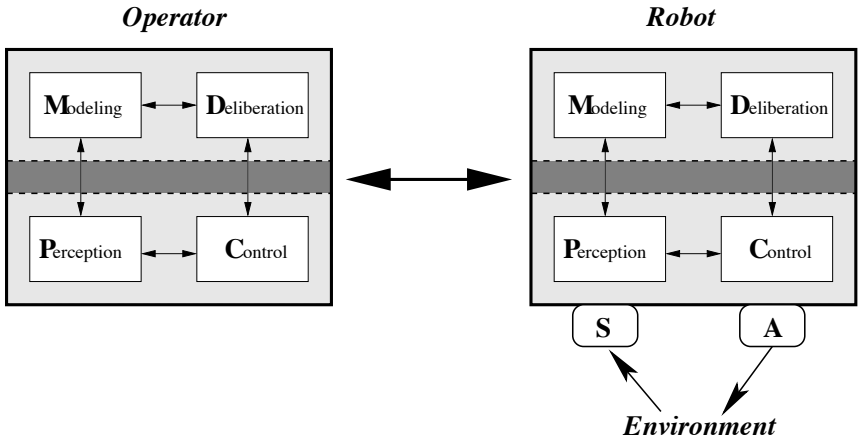

Figure 1.8: Shared autonomy diagram, demonstrating operator-robot cooperation [42].

In the shared autonomy architecture the operator act as a resource for the robot, managing and processing information like any other system module. This enables the operator to compensate autonomy or processing limitations, but their decisions are not time-critical nor much communications dependent. Shared autonomy emphasizes robot-human interaction to focus the attention where it is needed [42]. Moreover, with this architecture robot plays an important role, preforming tasks autonomously and with a good reliability and providing useful information to the operator, rather than being the operator to give one-way orders.

1.4 Outline

This thesis is structured as follows. Chapter 2 reviews some of the most relevant projects with lighter-than-air vehicles and stablishes the state-of-the-art of the unmanned control systems and sensors. In Chapter 3 the platform for the UAV is developed, as well the mechanical components needed to operate the UAV. This Chapter addresses also the blimp statical and dynamic analysis. Chapter 4 addresses the autonomous navigation and remote sensing problem and the on-board control system development. The sensors capabilities and limitations are also discussed. The Chapter 5 addresses the algorithm and communications protocol development. There is presented the sensor data processing algorithms as well the low level hardware oriented algorithms. In Chapter 6 the UAS performance is discussed and are presented the flight results and particular components performance. Also traced some objectives and guidelines for future projects are defined.

Chapter 2

Previous Work

For quite a while there has been some effort that aims the development of UAV platforms; some result from academics projects and others have commercial proposes. More recently, there has been an increased interest in controllable unmanned airships for aerial inspection platforms due to their stability properties and higher flight endurance [10].

This chapter presents the most relevant projects designed for surveillance and inspection missions based on LTA nonrigid airships, by highlighting the strongest and weaker features of the platforms used, control system hardware, sensing strategies and path-planning algorithms. This analysis is used as support for vehicle's design concept and aids in the selection of the sensors and techniques to solve the remote operation issue.

More recently, a new phenomenon has appeared in the UAV scene: the open-source hardware and software. These open-source projects and communities were used mainly to help define the state-of-the-art of aerial robotics. These communities are composed mainly by radio controlled (RC) hobbyist engineers that want to make their planes fly by their own. These communities provide useful data and feedback for commercial-off-the-shelf (COTS) sensors and hardware. Sometimes they can be also useful to search information concerning a particular problem.

2.1 Research and development projects

There are several research projects such as DIVA and AURORA. The DIVA project uses a nonrigid airship of 9.4 meters long as a platform for research in the areas of robotic integration, navigation and guidance, and vision based surveillance [21].

This project relies on several sensing devices like IMU, GPS and wind sensor, to provide information to the control system, but the vision plays an important role. The permanent pilot act as an emergency state, when the airship control system fails.

The control system implemented in this project is powerful, imaging processing and storage task require high CPU times and storage capacity. With the augmented processing power comes the increased weight and energy consumption which consequently leads to more weight. So, not surprisingly, the envelop used stores $18m^3$ of helium, providing more than $20kgf$ of lifting force. This project highlights the trade-off that needs to be established between the size, that influences directly the manoeuvrability and functionality of the UAV, and the hardware carried. Figure 1.2d depicts the DIVA airship where it is

possible to view its scale when compared to the surrounding people.

This vehicle has no sensors for object avoidance. The UAV flight characteristics and target missions – high altitude flights – disguise the lack of an object avoidance system. But these limitations affect the UAV working area since the pilot has always to maintain visual contact with the airship.

The AURORA project – Autonomous Unmanned Remote mOnitoring Robotic Airship – aims to develop an unmanned robotic airship capable of autonomous fly over user-defined locations for aerial inspection and environmental monitoring missions [16]. The platform is a LTA nonrigid airship with 10.5 m in length and 3.0 m in diameter resulting in $34m^3$ of volume.

The project intend to develop sensing and processing infrastructures for control and guidance capabilities, the ability to perform mission with adaptive re-planning of mission tasks based on real-time evaluation of sensor information [19]. This project, focus on modeling, control, sensing and navigation capabilities required by LTA vehicles [19].

Similarity to the DIVA project, the AURORA is based on a large scale airship. Moreover, all other relevant projects in this field rely on large airships – often as large as 10 m – like the Lotte project in Germany [28, 18]; the French projects at LAAS/CNRS [29]; the STWing-SEAS Blimp Project [27] from University of Pennsylvania; and the EnviroBlimp from CMU [26]. This can be explained by their mission objectives and normally high processing performance needed to perform visual based navigation.

In the sensing category the same solutions are almost unanimous adopted by all research teams. The AURORA incorporates GPS with differential correction, an IMU, one wind sensor at the nose and a vision system mounted on the airship's gondola. The wind sensor – built by IDMEC/IST – measures the relative airship air speed in all three axes, the aerodynamic incidence angles, as well as the barometric altitude [16].

Table 2.1: Review of sensors used in other projects.

Objective	**DIVA**	**AURORA**	**LAAS/CNRS project**
Attitude estimation	IMU	IMU	compass/inclinometer
Positioning	differential GPS	differential GPS	GPS
Environment sensing	wind sensor	wind sensor	wind sensor
	vision	vision	stereo vision
Object avoidance	–	–	–

Besides the sensors used to cover particular needs of the UAV platform, such as wind sensors commonly used in LTA vehicles, due to their hight sensitivity to winds gusts, but barely seen in other types of UAVs, the sensors used to navigate and positioning are well known and employed in almost all UAVs. The most common configuration is an IMU aided by a GPS system. A complete IMU is composed by three axis accelerometer, three axis gyroscopes and a three axis magnetometer. Some budget restrictions can limit the full employment of these sensors, but this affects the accuracy of the attitude and position estimator and the number of degrees-of-freedom (DOF) measured.

2.2 Commercial solutions

More than 400 different commercial solutions are available on the market, provided from more than 150 manufacturers [12]. The offers range from autopilots to implement in unmanned aerial vehicles to full featured platforms designed to accomplish specific tasks, these solutions vary greatly in flexibility and price. The range of UAV platforms models extends from micro-UAVs with a 15 cm wingspan and a payload capacity of a few grammes, to UAVs with a wingspan of 35 m and a payload of 2000 kg.

These projects are normally conceived to execute a pre-determined task, but do not provide the flexibility required for a research platform.

The most remarkable of these projects are the Draganflyer X6 from Draganfly Innovations, all the offers from AeroViroment, and the autopilot solutions: the MicroPilot , the attopilot and the kestrel from Procerus. Some of these projects are well developed and are the result of years of field experience.

The companies Draganfly Innovations and AeroViroment develop solutions to government agencies, universities and technical institutes around the world. The AeroViroment has an extensive portfolio of unmanned aerial vehicles developed to the US army, in which the Raven is included (figure 1.5). These platforms are quite advanced and offer many customizations, but their costs easily overcome the 20000€ barrier.

2.2.1 MicroPilot®

Micropilot develops autopilots for unmanned aerial vehicles and micro aerial vehicles (MAV), these solutions are open architecture and Micropilot provides the full documentation to the end user. The control board comes fully integrated with 3-axis gyroscopes, accelerometers, GPS, pressure altimeter, airspeed sensors, all packet into a board that weights only 28 grams. Figure 2.1 depicts the MP2028 autopilot system.

Figure 2.1: The MP2028 UAV autopilot solution from MicroPilot.

Like all commercial solutions, these autopilots are expensive, their price can reach 8000$ for the autopilot itself. MicroPilot also sells complete UAV airplanes starting at 9.5 k$ for the UAV only and up to 13.4 k$ for a UAV and ground station.

2.2.2 AttoPilot

The Attopilot auto-piloting system offers powerful but also function limited solution, being the less expensive commercial solution found with an price of $800. This was designed to be easily incorporated by RC hobbyists in to their planes, to control the servos, thus, allowing a low flexibility to add new sensors or to control other actuators. This accrues from closed source algorithm and from the servo oriented output method. The robot pose is given by thermopile-based sensors; as discussed in section 4.1.1, these systems are less effective when compared to gyroscopes.

2.3 Open source projects

This survey would be incomplete without mentioning the open source projects.

The open source community around UAVs is growing, and they constitute a great start point for anyone who wants to get involved and develop a UAV. These open source hardware and software projects offer great flexibility.

Open source projects differ among their community size and objectives. Some projects are based on a blog on which the author posts his achievements and gives advices about sensors performance and control techniques. Others, like the DIY Drones [7], have a more active community and involve more people and manufacturers; this particular community has several amateur UAV projects developed with the arduino open hardware architecture.

These projects result from the work of one group of people that has same objective. These goals vary from the development of a customizable open source UAV flight control systems [7, 2, 3]. To a fully functional UAV [45, 1] and others are more focussed on the development of graphical interfaces and test software, based on hardware in loop simulation [24, 40].

Figure 2.2: The UAV DevBoard, an three-axis autopilot development board developed by Bill Premerlani.

One thing that all of these projects have to struggle with, is to develop a fully functional solution with limited resources.

The UAV Devboard autopilot (figure 2.2) comes with a dsPIC from Microchip running at 120 MHz, 3 axis accelerometer and 3 axis gyroscopes.

It was developed for the do-it-yourself projects, can be also used to develop a three axis inertial measurement unit (IMU) controller. This board has several input and output ports to communicate with external sensors and actuators.

This autopilot is a great alternative to commercial products, and costs $150 from SparkFun. Besides not being a complete solutions this board still offers the best price to functionality ratio, from all the solutions analysed.

Chapter 3

System Design

This chapter introduces the conventions and assumptions made to preform the static and dynamic analysis. Then follows the description the overall design concept for the platform and components selected.

Finally the static and dynamic study are presented, making some conclusions concerning the flight characteristics of the blimp. Thus this chapter address the development of the UAV platform.

The reference axis for blimp displacements and rotations is defined according to the figure 3.1. To define the attitude of the Blimp it was used some conventions of aeronautics: the Euler angles are used in the formulation of this model (ϕ, θ, ψ) – roll, pitch and yaw.

The linear displacements (x, y, z) and orientation angles (ϕ, θ, ψ) in the blimp center of gravity (CG) axis, are usually considered as state variables. Figure 3.1 depicts the positive directions used in this thesis.

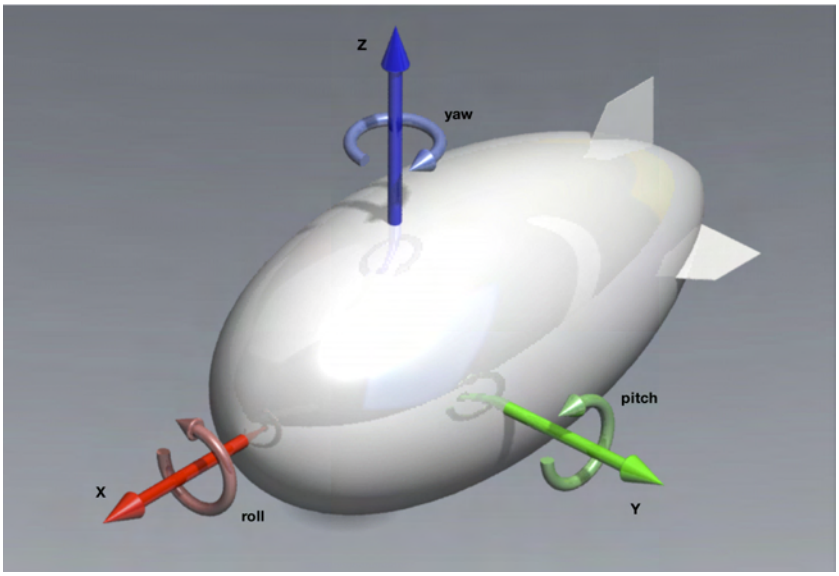

Figure 3.1: Reference axis considered, for future analysis.

3.1 The UAV platform

After discussing which platform is more adequate for this thesis goals, were clear that the helicopter and LTA platforms are the ones that offer the best arrangement between functionality and disadvantages, due to their unmatched hover and VTOL ability.

As highlighted when defining the objectives (section 1.2) the robot most provide a satisfactory autonomy, robustness with a proper price. So for this project, the lighter-than-air airship was chosen. It was found that an helicopter based platform would inevitably lead to a shortened flight endurance, higher cost and, not less important, the control algorithm would have to be more complex and susceptible to misbehaves.

This particular type of VTOL can achieve more flight endurance and due to the fact that this vehicle is inherently stable, simpler control algorithms are needed. This characteristic also ensures that the robot is not damaged in the event of a system failure. Lighter-than-air vehicles also makes UAS cheaper and requires less maintenance in opposition to other types of VTOL aerial vehicles.

There are commercial LTA vehicles, that could be used for this project. Advertisement blimps solutions offer a wide range of blimp sizes, from 2.2 meters indoor blimps to 16 meters long outdoor blimps. Hobbyist radio controlled solutions were too small, typically under 1.2 meters long, these are purely indoor vehicles, and don not suit the needs of this project. Complete radio controlled advertisement solutions are fitted with functionalities and components designed specifically to advertisement purposes and as exposed in section 3.2.2 have some limitations. Moreover, these fully featured vehicles are costly, starting at 2000€ and reaching 5000€ for a 6 meters long blimp.

So we decided that it was best to develop a custom platform specifically designed for the goals of this project.

3.2 Blimp design

Lighter-than-air aircrafts are the simplest way to produce a controlled flight; they have few moving parts that require fewer maintenance than other types of VTOL aircrafts. Moreover, in almost all radio controlled indoor blimps the only moving parts are the propellers.

Blimps are composed by: an envelop, a thin polymer container for the gas; a gondola, attached to the bottom of the envelop, where the control systems and batteries are kept; and also by actuators, that can consist of two thrusters to provide front movement and one tail thruster to control the heading direction. All these components can be seen in figure 1.3 on page 6.

3.2.1 Envelop

The envelop is, apparently, the simplest component of a blimp, but it is the most important part. It largely influences the characteristics of the UAV and the performance in indoor and outdoors flights.

Selecting the right size is one of the most crucial decisions during the conception of the vehicle. The envelop needs to be large enough to provide buoyancy to lift all the components and electronics, but yet it is intended that this vehicle has some level of manoeuvrability indoors and thus limiting the dimensioning of the envelop. On the other hand, to fly the blimp outdoors, bigger motors are needed to cover for wind gusts, which also leads to a bigger envelop. So, a trade-off needs to be made between the ability to flight indoors and outdoors.

The selected envelop spans three meters long and the cross section has a maximum diameter of 1.4m, granting a total volume of 2.9 m^3 (figure 3.2). This choice was made after making an estimate of the weight of components to be used and the ability to transport some additional payload. As expected the considerable large dimensions of this envelop, limits its application in indoor flights. The large dimensions of the envelop reduces also its dexterity in constrained outdoor areas.

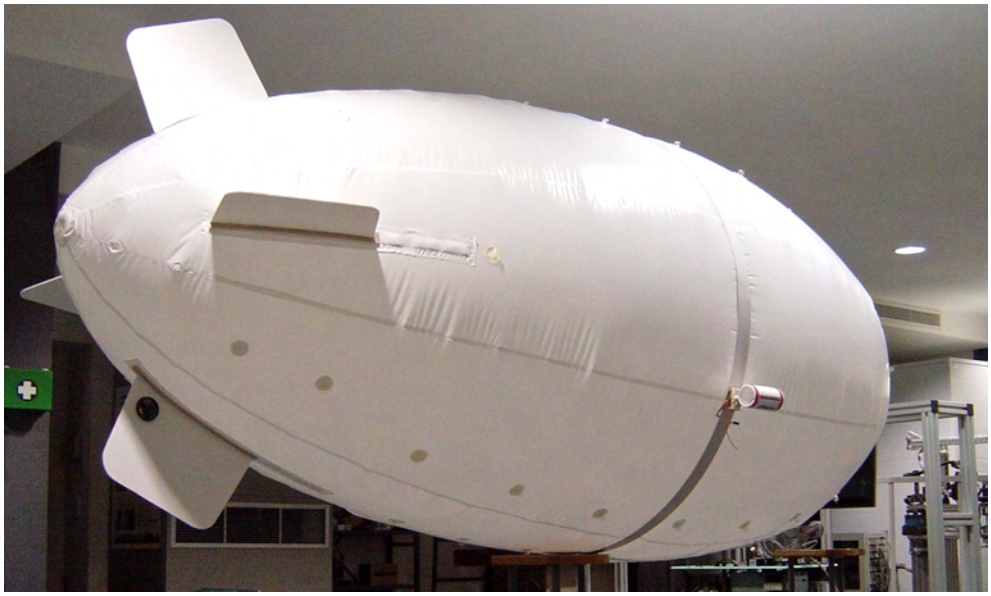

Figure 3.2: A photograph of the envelop filled with helium, in the LAR.

This envelop is sold by Hangzhou Chiny Aircraft Technology Co, and has the following characteristics, displayed in table 3.1.

Table 3.1: Envelop general characteristics.

Envelop	
length	3.0 m
diameter	1.4 m
volume	2.9 m^3
weight	1189.5 kg
maximum speed	40 $km.h^{-1}$
flight altitude	5-20 m

3.2.2 Propulsion

For structural reasons, the thrusters are normally placed in the lower part of the blimp, attached to the gondola. This simple approach, with few moving parts and keeping the thrusters close to the gondola, decreases the risk of failure but also limits the manoeuvrability of the vehicle. The thrusters, in this configuration, tend to produce pitching moments when significant thrust forces are applied, making the Blimp balance in high accelerations or decelerations.

In order to reduce this behaviour, in this project, the thrusters will be placed as close as possible to the center of gravity, in the X and Z dimensions. The thrusters positioning and the CG of the blimp are seen in figure 3.3. In this position the thrusters are placed near the maximum cross section of the envelop, increasing the distance between the engines. This positioning affects positively the manoeuvrability, increasing the effectiveness of the thrusters in turning manoeuvres.

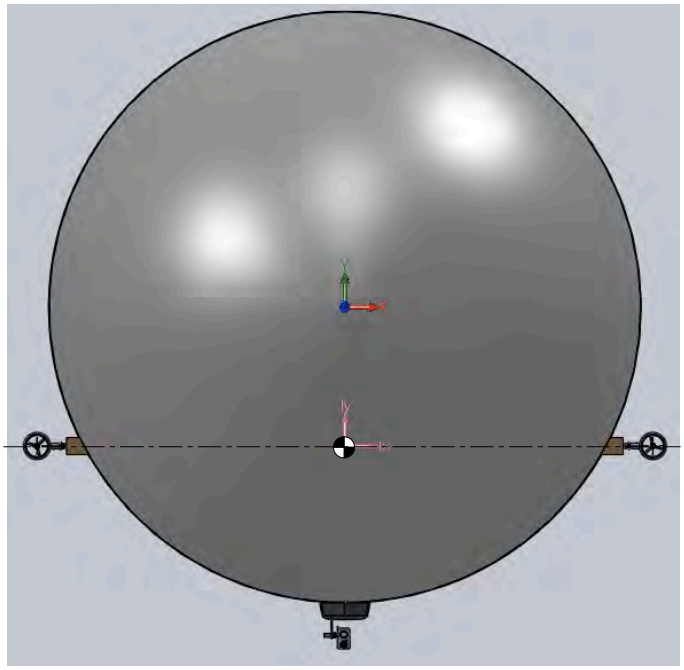

Figure 3.3: Illustration of thrusters positioning in relation to CG and the centre of lift.

The use of electric motors combined with ducted fans grants important capabilities, such as, reduced acoustic signature, smaller size, granting an increased effectiveness in persistent intelligence, surveillance and reconnaissance (ISR) missions. The duct reduces propeller blades tip losses. The ducted fan produces thrust more efficiently than a conventional propeller, by reducing the tip vortices of the propeller and directing its thrust towards the back only.

The propulsion is granted by three ducted fans with 51 millimeters of diameter. Table 3.2 summarizes the ducted fans specifications. These ducted fans are powered by brushed DC motors and, when operating at maximum voltage (12 volts), they generate 130 *grams-force* of thrust.

Two ducted-fans are used as vectoring thrusters and are placed on the lateral of the envelop. These orientable thrusters provide mainly control over the X and Z axis move-

Table 3.2: Thrusters characteristics.

Ducted fan with N60 motor.	
weight	30.2 g
thrust	130 gf
Max voltage	12 volts
Loading current	5.5 A

ments, but are also able to turn the blimp, when operating at different loadings. The third ducted fan is placed in the tail, and assists in turning manoeuvres. Figure 3.4 shows the proposed vectoring thrusters system.

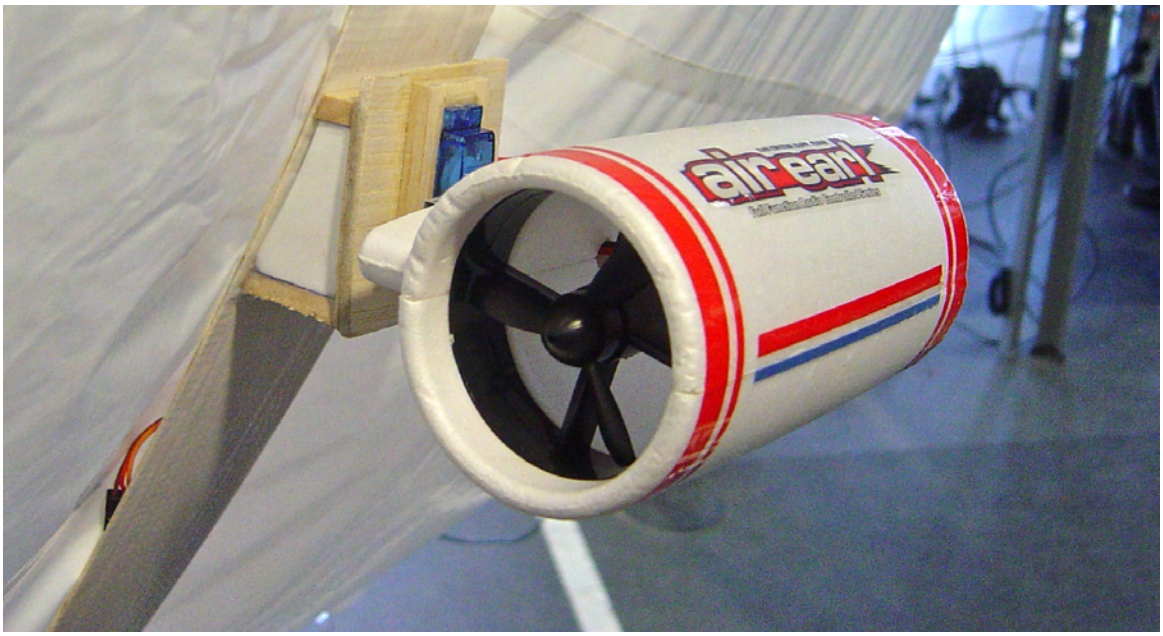

Figure 3.4: Render of the ducted fan based propulsion system developed.

Servo motors to orient the thrusters

In this section we will design and study the performance of the servo motors, that are responsible for tilting the thrusters.

There are three forces induced by the ducted fans on the servo bracket (figure 3.5): the ducted fan weight; the thrust produced; and the aerodynamic force. As the figure 3.4 depicts, the servo is placed on the geometric center. This implies that two of the forces – the thrust and the aerodynamic – have no moment effect on the servo bracket.

The opposing moment created on the servo bracket is maximum when the ducted fan is in the horizontal position, and the servo starts moving the fan clockwise. In this position the servo output torque needs to overcome the moment created by the mass plus the inertial moment; the moment is then given by the equation 3.1.

$$\Sigma M = I \times \alpha + w \times r \tag{3.1}$$

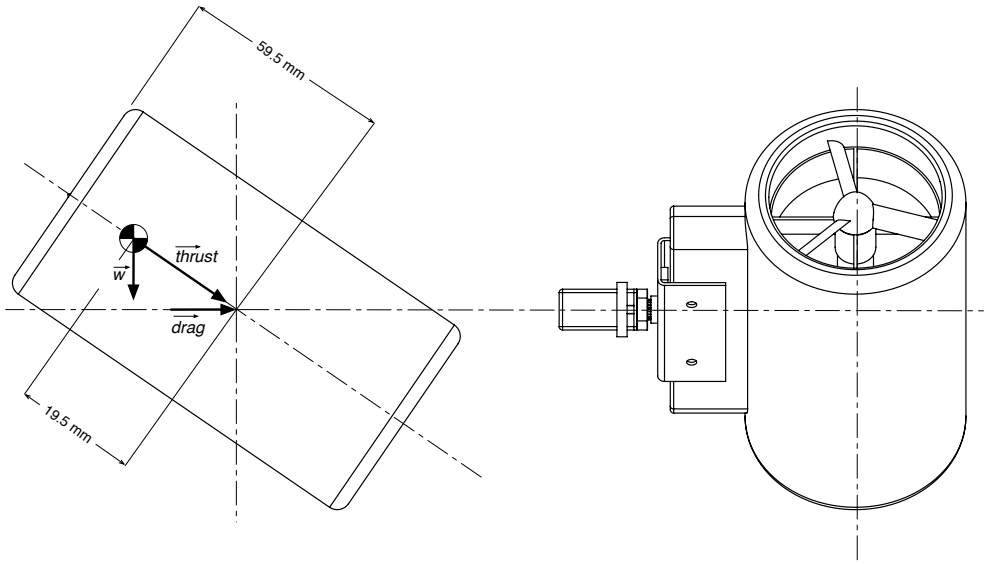

Figure 3.5: Free-body diagram of the loads acting on the servo bracket.

where, I denotes the thruster rotational inertia, α the angular acceleration associated with the movement, w the ducted fan weight (represented in the free-body diagram of figure 3.5), and r distance between the thruster CG and the rotational axis (figure 3.5).

The servo selected was the Turnigy TG9 micro servo which weights 9 grams and is displayed in figure 3.6. This servo is capable of generating 1.6 kg.cm of torque and rotates at 8.72 rad.s^{-1} (with no load applied). One initial static analysis to the servo prove that almost any servo can deal the task. This servo offers a good price to performance ratio, ensuring also a good factor of safety (FOS).

Figure 3.6: Servo motor used, from Turnigy.

Being a position controlled servo, the only parameters that are granted by the servo are its angular position and the maximum torque. Then the rotational movement properties that this servo can ensure will be studied, more specifically in the critical situation, described by the expression 3.1, which occurs when the ducted fans are in the horizontal position and when the control commands orders the servos to rotate clockwise.

Considering the ducted fan as a concentrated mass displaced 19.5 mm of the rotational

center, its moment of inertia can be determined by the equation 3.2.

$$\begin{aligned} I &= m \times r^2 \\ &= 30.20 \times 19.5^2 = 114.84\ g.mm^2 \end{aligned} \tag{3.2}$$

Solving for the angular acceleration after equation 3.3; where, the former member represents the servo torque in N.m and the latter the sum of the rotational inertia and the moment created by the fan weight, both converted to N.m, results in the following:

$$1.6 \times 10^{-2} \times 9.81 = 114.84 \times 10^{-9} \times \alpha + 30.20 \times 9.81 \times 19.5 \times 10^{-6}$$

$$\alpha = 13.169 \times 10^3\ rad.s^{-2}$$

The magnitude of the theoretical acceleration provided by the servo highlights its good FOS; the moment created can easily overcome the angular inertia with a quick acceleration.

There are no manufacturer information regarding the maximum shear stress supported by the servo bracket. Yet, this will be studied to grant that the tensile strength of the TEFLON, formerly PolyTetraFluoroEthylene, is not exceeded . PolyTetraFluoroEthylene is commonly abbreviated PTFE and supports a shear stress up to 11.7211 MPa [41] (expression 3.3).

$$\tau = \frac{F}{A} \tag{3.3}$$

The maximum aerodynamic force occurs when the fan is in the vertical position, due to the larger area projected on the air stream normal plane. The maximum shear stress also occurs in the vertical position, when the thrusters are faced down; in this position the thrust and the fan weight have the same direction.

The drag force was determined according to equation 3.14, on page 30, with $C_D = 0.3$ [9] – drag coefficient of an cylindrical body – and for the maximum velocity determined in equation 3.21:

$$drag = \frac{1.204 \times 10.13^2 \times 0.3 \times 119 \times 65 \times 10^{-6}}{2} = 0.287N \tag{3.4}$$

The stress then is determined from the vectorial sum of all vectors, (equation 3.5). The servo bracket has 3 mm of diameter.

$$\tau = \frac{\sqrt{((w + thrust)^2 + drag^2}}{A} \tag{3.5}$$

$$\tau = \frac{\sqrt{((0.030 + 0.130) \times 9.81)^2 + 0.287^2}}{\frac{\pi \times (3 \times 10^{-3})^2}{4}}$$

$$\tau = 0.116MPa$$

The previous analysis allows to conclude that none of the servo limits will be exceeded during the normal operation of the UAV. This light-weight servo grants good acceleration and torque for the vectoring thrusters solution.

3.2.3 Gondola

The gondola is placed below the envelop and needs to be easily removed, or grant easy access to the electronics, battery, and payload compartment.

The gondola is responsible to accommodate and protect the electronics systems and the payload. It will have to be as light as possible but stiff enough to withstand payload, that can weight up to 976 g (section 3.4).

The gondola will have an internal structure in balsa wood that will be covered by a thin thermoplastic layer. The balsa wood has low density, which makes it a good material for light weight applications. Its simplicity to machine and mold make it easy to use and manipulate.

The plastic cover is mainly used to reduce the drag and to protect the electronics from adverse weather conditions. Figure 3.7 depicts the gondola proposed, and the respective internal structure.

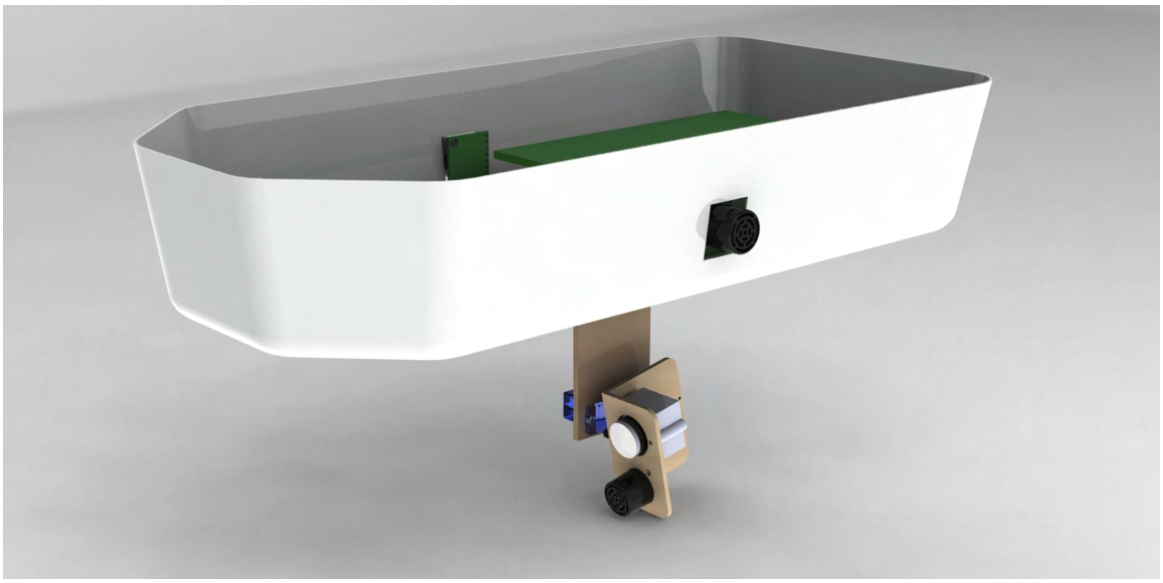

Figure 3.7: The custom designed gondola.

3.3 Power supply

The electric motors are powered by Lithium-ion Polymer batteries, these batteries have the best energy to weight ratio among all other types of rechargeable batteries. Each Li-Po cell has a nominal voltage of 3.7 V. To fully take advantage of the thrusters will be installed a 3 cells package, delivering 11.1 volts.

To size the battery pack, it will be consider that on a normal flight, the ducted fans will operate at an average of 20% of their capacity, and the rear thruster will be active at full power 5% of the time. With this load profile, the continuous current drained by the three motors is 2.25 A. This load profile results from the knowledge gained from previous blimp experiments. The thrusters load will vary greatly with the mission, but the first flight test will be used to verify these assumptions.

The control and motion systems are all powered from the same battery. The voltage is regulated to 5 Volt and then to 3.3 Volt, the electronics systems – including the three servos and the LED – drain 950 mA at 5 Volt. The total power consumed by the robot during the flight is determined in the expression 3.6:

$$\begin{aligned} P &= V \times I \\ P &= 11.1 \times 2.25 + 5 \times 0.95 \\ P &= 24.97 + 4.75 = 29.72\ Watt \end{aligned} \tag{3.6}$$

where P denotes the power drained, V and I the voltage and current flowing trough the circuit.

The batteries were sized to enable a flight endurance of one hour in the previously mentioned conditions. The total energy needed to flight the blimp for 60 minutes is given by the expression 3.7, the energy is converted to Wh, to simplify the selection of the battery pack. Equation 3.8 indicates the minimum capacity for the battery pack.

$$E = P \times 1\,[hours] = 29.72\ W.h \tag{3.7}$$

$$Capacity_{min} = \frac{29.72}{11.1} = 2678\ mA.h \tag{3.8}$$

3.4 Blimp static analysis

The buoyancy generated for cubic meter by the helium is given by equation 3.9, and results from the difference of densities from this two fluids – the helium and air proprieties at standard conditions for temperature and pressure (SPT) are summarized in table 3.3 [34].

Table 3.3: Air and helium density, their specific constant and dynamic viscosity properties at sea level and 293.15 K.

Property	Value	
ρ_{air}	1204.200	$g.m^{-3}$
R_{air}	187.050	$J.Kg^{-1}.K^{-1}$
ρ_{He}	166.250	$g.m^{-3}$
R_{He}	2079.020	$J.Kg^{-1}.K^{-1}$
μ_{air}	0.018	$mPa.s$

The envelop has a total volume of 2.9 m^3. The helium contained inside the envelop, produces 3.01 kgf of lift, equation 3.10, at SPT conditions.

$$Buoyancy = 1204.20 - 166.25 = -1.038 \frac{kgf}{m^3} \quad (3.9)$$

$$Lift = 1.113 \times 2.9 = 3.010\ kgf \quad (3.10)$$

To that gross value of lift, needs to be subtracted the weight of all components necessary to operate the vehicle. The component weights where measured and the results are in table 3.4, there's 976 grams left to accommodate payload and ballasts.

Table 3.4: Component weights, and the payload capacity left.

Component	**weight (g)**
Envelop	1189.50
Thrusters	146.23
Batteries	200.10
Gondola	572.00
Electronics and sensors	486.00
Payload left	316.17

It's important to inflate the envelop with the same surrounding conditions that the blimp will face during the mission. Changes in environment temperature and pressure influence the blimp lift capacity and the envelop shape and integrity.

With an external pressure drop the global lift will decrease. The envelop keeps the same volume leading to an inside overpressure that decreases the lift, and ultimately can lead to an envelop rupture.

The temperature also affects the lift capacity. Temperature rises affect the density of the two gases differently. This fact, and already considering that the pressure inside the envelop was corrected to the surroundings pressure, can lead to a decrease of buoyant lift.

The gases density can be determined by the equation 3.11.

$$\rho = \frac{Pressure}{R \times Temperature} \quad (3.11)$$

where the *Pressure* is in Pascal, the *Temperature* in Kelvin, and R denotes the specific constant of the gas and is presented on table 3.3.

An accurate computation of buoyant lift needs to take into account the vehicle altitude, relative humidity, and internal envelop pressure above the ambient. The helium temperature may also be 10ºC or more above or below the ambient air – this is caused largely due to heat absorption or radiation by the envelop [31].

For this analysis only the temperature oscillations were taken into account; altitude and pressure differences between the helium and the outer air were neglected due to the particular target missions. The simulations were made in MATLAB environment and the results are stated in figure 3.8. At 30ºC, the total lift produced by the blimp will drop 330 *grams-force*, in comparison to a winter day with a room temperature of 0ºC.

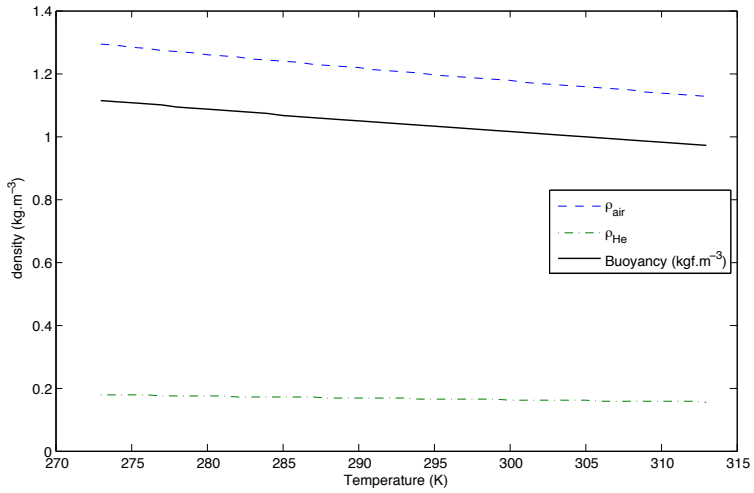

Figure 3.8: Specific gas volumes variation with temperature, and specific buoyancy produced.

3.5 Flight dynamics

This section addresses the blimp flight characteristics analysis. In sections 3.5.1 and 3.5.2 are calculated its maximum acceleration and velocity, respectively. Then, in section 3.5.3, the study the evolution of these parameters in different flight conditions is presented. Is also drawn some considerations regarding the maximum operating wind speeds, section 3.5.4. All these characteristics are summarized on table 3.6 on page 36.

Low-cost radio controlled blimps have one vertical propeller to control altitude, but that is not effective enough to keep the blimp under control, unless the blimp is exactly trimmed and weather conditions do not change [6]. The best way to increase the vertical response is to tilt up or down the main thrusters – the vectoring thrusters. This is a very straightforward solution, but in terms of control it can be more complex, since the vertical and the horizontal movements are related to each order.

The blimp is controlled by two vectoring thrusters and a third tail thruster to help control the blimp in narrow turns. One of the main advantages of lighter-than-air vehicles are the inherent stability of some degrees of freedom (DOF), in terms of control this is translated in the non-necessity of control over this particular DOF. Like any object moving in the 3D plane, this robot has six DOF to consider, shown in figure 3.1, yet only four of the six flight parameters can be controlled. It's assumed that the roll and pitch are invariable, and auto-stable, during the flight.

The robot uses three DOF to control these four flight parameters – the position of the vehicle over the three coordinate system (x, y, z) and the heading direction (ψ). The control system has control over the following DOF: the thrust produced by the ducted fans (T); the tail fan thrust (t_{tail}); and the vectoring thrust angle (θ). This control can not be preformed independently, and the Y coordinate results from the composition of two other parameters (x and ψ); the system that describes this transformation is found with expression 3.12 (considering that no external forces, like wind gusts):

$$\begin{cases} x &= f_{x(\cos(\theta),\ T)} \\ y &= f_{y(x,\ \sin(\psi))} \\ z &= f_{z(\sin(\theta),\ T)} \\ \psi &= f_{\psi(T_{tail})} \end{cases} \tag{3.12}$$

where can be seen the relationship between the DOF and the robot attitude and position. Note that the arguments considered are just the ones that can be controlled, others can influence the final result, like the wind. T denotes the thrust of the ducted fans; θ the tilt angle (according to the figure 3.5); ψ the heading angle; and T_{tail} denotes the thrust produced by the tail thruster.

The system path planning outputs three coordinates and one attitude indicator (x,y,z,ψ). The motion control unit actuates the 3 DOF (T,θ,T_{tail}) to lead the vehicle to the correct coordinates and with the attitude desired. Since the two sides can be independently controlled, the robot can have up to 5 DOF (T_{right},T_{left},θ_{right},θ_{left},T_{tail})

3.5.1 Acceleration

The acceleration that the blimp is capable to generate , is determined in equation 3.13, this approximation is only valid for initial period of the movement, when the velocity is low, and the drag forces can be neglected. The two thrusters generate a maximum of 2.55 N of thrust.

$$\begin{aligned} a &= \frac{Thrust}{w_{UAV} + w_{He}} \\ a &= \frac{0.130 \times 2 \times 9.81}{3.01 + 0.166 \times 2.9} = \frac{2.55}{3.49} = 0.73\ m.s^2 \end{aligned} \tag{3.13}$$

The mass of the vehicle results from the total mass that can be lifted by the helium plus the mass of the helium it self.

3.5.2 Maximum velocity

The maximum velocity is achieved when the drag force equals the thrust, this equilibrium is represented by the system of equations 3.14 [30, 9] and can be seen graphically in figure 3.11 on page 33.

$$\begin{cases} Thrust &= \frac{1}{2} \times \rho_{air} \times A_{fan} \times ({v_{out}}^2 - {v_{in}}^2) \\ Drag &= \frac{1}{2} \times \rho_{air} \times v^2 \times C_D \times A_{blimp} \end{cases} \tag{3.14}$$

Where ρ_{air} represents the air density, A_{fan} and A_{blimp} represent the effective fan and the blimp frontal areas, respectively; ${v_{out}}^2$ the velocity of the air stream leaving the ducted-fan;

${v_{in}}^2$ and v^2 represent the blimp relative air speed, and C_D the blimp drag coefficient.

The thrust generated by the propeller is a result of the difference of pressures between the front and back sides of the propeller, caused by the acceleration of the air through it. The thrust is given by the effective area of the circle that the propeller creates while rotating. The effective area is given by the area of the circle that the blades describe when rotating, without the inner and outer sections (figure 3.9). The contribution of these sections to the thrust is small, due to the vortices created at the blade tips, and the low velocity of the inner section.

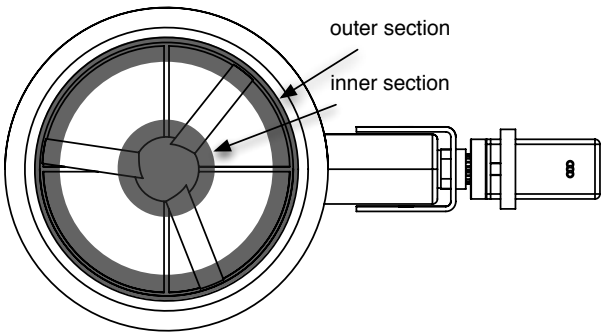

Figure 3.9: Representation of the ducted-fan effective area.

Applying the Bernoulli's equation to the air stream [30] passing through the fan, results in the equation 3.15, which gives the thrust produced:

$$Thrust = \frac{1}{2} \times \rho_{air} \times A_{fan} \times \left({v_{out}}^2 - {v_{in}}^2\right) \tag{3.15}$$

where, A_{fan} is the effective area given by the equation 3.16.The effective area result from the area associated with the blades diameter L, without the inner (L_{inn}) and outer (L_{out}) sections.

$$A_{fan} = \pi \frac{L^2 \times \left((1 - L_{out})^2 - {L_{inn}}^2\right)}{4} \tag{3.16}$$

The steady thrust produced by each of the ducted fans is 130gf, so starting with the expression 3.15, the velocity of air the exiting the ducted fan can be determined by expression 3.19.

$$v_{out} = \sqrt{\frac{0,260 \times 9.81 \times 2}{\rho_{air} \times A}} \tag{3.17}$$

where, A is obtained by expression 3.16, considering an inner loss of 10% of the diameter and no outer loss. Due to the ducted fan characteristics, addressed in section 3.2.2, the outer loss was neglected.

$$A = \frac{\pi\left(51 \times 10^{-3}\right)^2\left((1-0)^2 - 0.9^2\right)}{4} = 1.655 \times 10^{-3}\ m^2 \tag{3.18}$$

then the velocity of the air living the ducted fan is given by, equation 3.19.

$$v_{out} = \sqrt{\frac{0,260 \times 9.81 \times 2}{1.204 \times 1.655 \times 10^{-3}}} = 48.84\ m.s^{-1} \tag{3.19}$$

The drag coefficient of a 3-D streamlined body is dependent of the fitness ratio – ratio between the length of the body and its thickness – and the Reynolds number [9]. Given the fitness ratio of 2.14 (equation 3.20) results $C_D = 0.030$ – visually measured from the graph of the figure 3.10 [9].

$$\textit{fitness ratio} = \frac{3}{1.4} = 2.14 \tag{3.20}$$

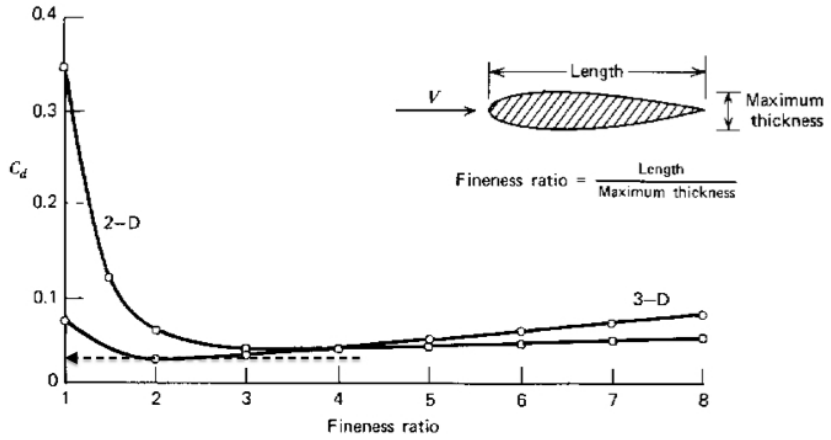

Figure 3.10: Drag coefficients for streamlined shapes as a function of fitness ratio. C_d based on frontal area; R-10^7 based on length [9].

Now all the information needed to solve the initial system is known the maximum velocity can be determined. Starting with the system of equations 3.14 and making some simplifications results in the equation 3.21, which allows the calculation of the equilibrium velocity. Where ${v_{in}}^2$ and v^2 are now denoted by v_{max}^2, which represents the blimp maximum velocity.

At the maximum section the envelop has 1.4 metres of diameter, resulting the frontal area of $1.54m^2$.

$$v_{max}^2 = \frac{v_{out}^2}{\frac{C_D \times A_{blimp}}{A_{fan}} + 1} \tag{3.21}$$

$$v_{max} = 9.08\ m.s^{-1}$$

To validate the previous calculations the Reynolds number must be determined, equation 3.22. The drag coefficient is dependant of the Reynolds number, and the graph used is only valid for Reynolds numbers of the 10^7 magnitude.

$$R_e = \frac{\rho \times V \times L}{\mu} = 1.761 \times 10^7 \tag{3.22}$$

The Reynolds number is within the range of the requirements for the drag coefficient analysis.

3.5.3 Blimp behaviour

The maximum flight characteristics were determined to specific regimes that constrain their maximum value. But these parameters vary with different flight regimes. This information is relevant to implement, in future works, real-time simulations tools based on Hardware-in-the-Loop Simulation (HILS) software, where the physical parameters and response need to be known.

The thrust and the acceleration that the thrusts can impose in a given moment are inversely proportional to the relative air speed. As the blimp starts to move aerodynamic forces begin to act, lessening the effective thrust. Increasing the UAV velocity the thrust decreases due to the reduction of the difference of pressures (equation 3.15).

These dependences are stated in 3.11, that results in the figure 3.12, where the acceleration variation with the relative air speed is presented. Figure 3.11 depicts the equilibrium point, that allowed to determine the maximum velocity and is characterized by the equilibrium between the two forces.

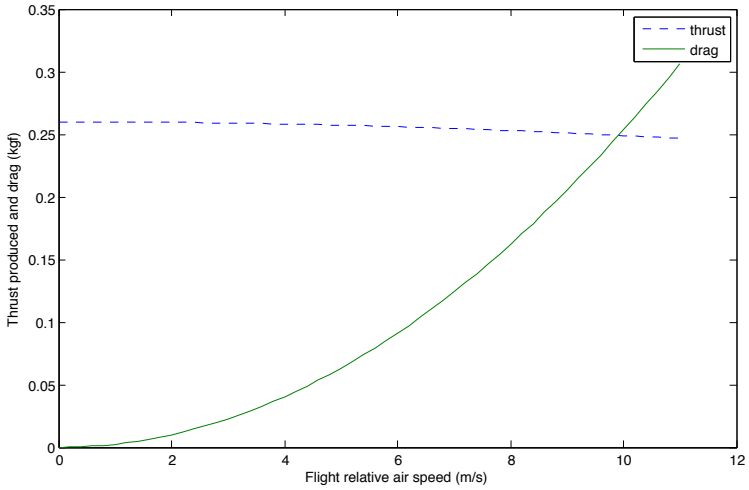

Figure 3.11: Dependence of thrust and drag with the UAV velocity.

3.5.4 Maximum operating winds speeds

For security reasons the maximum operating winds speeds will be calculated. This was achieved considering the maximum frontal winds that the thrusters can compensate and

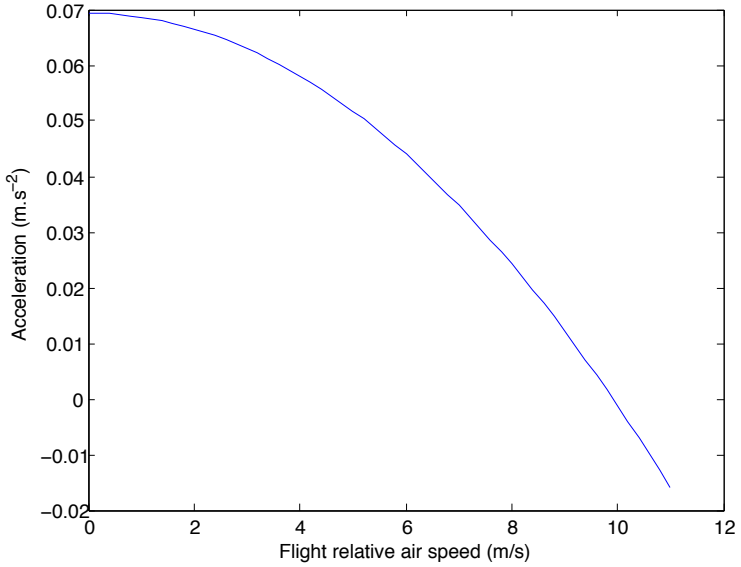

Figure 3.12: Acceleration variation with UAV velocity.

the maximum crosswinds ratings – to enable the blimp to correct the position deviation in a specific given time.

We have considered that a constant frontal wind speed of 30% of the blimp maximum velocity will be the top limit – in this type of conditions the blimp already has to make a significant effort to keep its position. Since the propellers do not have the same performance when rotating backwards, the tail wind resistance is slightly smaller. A maximum allowable wind speed of 20% of the blimp maximum velocity will be considered.

Since the blimp has no direct control over movements along the y axis and the larger lateral area of $3.15m^2$ turns the blimp less to tolerant to crosswinds. The vehicle is designed for low altitude flights close to buildings; in those cases, significant deviations can lead to collision and subsequently damage the blimp. These are the most dangerous missions preformed by UAVs and require an extreme and permanent attention from the operator.

As mentioned in Chapter 1, the UAV will have an integrated low-level sensing, based on sonar distance measurement sensors to prevent collisions; these sensors can measure distances up to $\approx$ 6 meters with an error of $\approx$ 2.5 cm. These sensors are discussed in section 4.1.4.

Considering an inspection mission to a building, at a constant distance of six meters, where the blimp must fly parallel to the side of the building. It will be accepted that the wind induce a maximum acceleration of 0.5 m/s^2 on the blimp towards the building, in this scenario the UAV only has about 3.5 seconds to escape from this situation.

The wind speed was determined based on the same logic used in previous calculations, expressions 3.13 and 3.14. The drag force will be substituted by the blimp inertia in the referred conditions, resulting in the following:

$$v_{crosswind} = \sqrt{\frac{2 \times w \times a}{\rho_{air} \times A \times C_D}} \quad (3.23)$$
$$= 1.75\ m.s^{-1}$$

where, A now represents the envelop lateral projection area; C_D is approximated to a drag coefficient of a cylinder in a turbulent regime (0.3); w denotes the blimp weight (3.75 kg)

Finally, the wind speeds allowed to flight the UAV outdoors are presented in table 3.5.

Table 3.5: Maximum operation ratings of wind speeds that the blimp can withstand and correct.

Property	**Value** ($m.s^{-1}$)
headwind	≤ 3.04
crosswind	≤ 1.75
tailwind	≤ 2.02

3.6 Platform overview

This section will summarize the results of the analysis made previously including the relevant performance characteristics of the blimp. Also, the components to complete the blimp structure are presented, although they do not have an important role to the blimp performance.

The platform is a LTA non rigid airship, with 3 m long, 1.4 m diameter and with a total volume of $2.9m^3$. It has a semi-rigid structure that supports the motors the gondola and distributes their weight, over an large surface of the envelop. This belt that embraces the envelop has 3.96m long and 5cm width, its made from a thin balsa wood stripe reinforced with bi-axial fibres, this can be seen in figure 3.13b. The vectoring thrusters implemented in the platform are depicted in figure 3.13c

The rear stabilizers, were made with a 2 mm thick balsa wood, covered with a transparent self adhesive plastic layer. The button stabilizer holds the rear thruster; once again this thruster is vertically aligned with the CG, producing yaw moments only. Figure 3.13a depicts the rear stabilizers manufactured, and the rear thruster.

Finally the fully assembled platform for unmanned aerial vehicles, is mentioned. Figure 3.13d highlights some design properties of the UAV platform developed.

The aerial platform developed has the following main flight characteristics (table 3.6).

(a) Rear stabilizers, and the rear thruster positioning in detail.

(b) Detailed view of the linking belt.

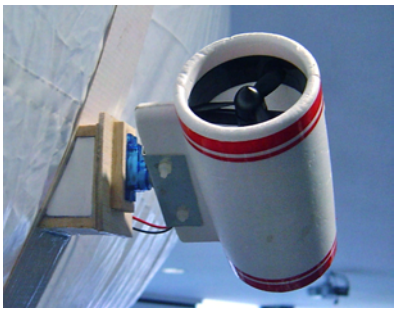

(c) Vectoring thrusters solutions in detail.

(d) Blimp platform developed, at LAR.

Figure 3.13: Blimp platform developed, with detailed views of particular solutions implemented.

Table 3.6: Blimp general characteristics and performance specifications.

Blimp	
length	3.00 m
width	1.48 m
payload	316.17 g
maximum velocity	3.04 $m.s^{-1}$
flight endurance	30 minutes
range	2.7 km
max. operating winds	see table 3.5

Chapter 4

On-board Systems

On-board control architectures for UAVs have to integrate a variety of sensorial information (geo-localization, aircraft attitude reference sensors, altitude sensors, among others), and low level motion servo-controllers, to operate the vehicle in different control modes. The on-board hardware is seriously constrained by the load, energy consumption and weight [39]. This situation is even more critical when developing control systems for LTA aerial vehicles.

This chapter addresses the autonomous navigation and remote sensing problem and establishes some objectives for the hardware responsible for navigation and vehicle control. Then, will be suggested on-board sensors to solve the position and attitude estimation problem; environment perception, obstacle avoidance and planning capabilities are also considered for sensor selection. In section 4.3, the on-board control hardware architecture is developed, integrating all sensors from section 4.1, including a wireless communication system to a ground station.

As established in the Objectives section, it is intended to design a control system flexible enough to enable the control of several types of vehicles, ground-based or airborne, with minor hardware and software changes. This control board will be based on low-cost micro-electromechanical sensors (MEMS), to provide the estimation of attitude angles and position, and monitor other flight and environment variables. Advances in MEMS enabled the development of low-cost inertial measurement technology in the last decade.

The adoption of commercial-off-the-shelf (COTS) sensors and communications solutions will be made when these sensors are commercially available and at a reasonable cost. This option will enable savings in development time and being more confident with the hardware used – where both the correctness of the results and their timely delivery must occur for the vehicle to be operated safely [43].

The control system relies on an inertial measurement unit including an accelerometer, a gyroscope and a magnetic compass. The state estimation is complemented with geo-localization information (GPS) and an altimeter.

To accomplish the objectives set for to the UAV, the control system must be able to provide:

- low-weight and low energy consumption;

- real-time telemetry;
- embedded safety systems;
- periodically read and process data from all sensors.

4.1 Sensor description

The sensors will be presented by their function or by the propriety they are designed to measure. Their functional principle, and their advantages and limitations will also be described in this section.

4.1.1 Attitude estimation

The attitude estimation is critical in indoor flights, where no GPS data is available. The robot attitude estimation is not a result of a single sensor data reading or processing, but instead a combination of sensors that together form what is commonly known as an inertial measurement unit (IMU). The attitude is defined by the Euler angles, as in figure 3.1 on page 19, and their determination is extremely important, specially for aerial vehicles, since it affects the vehicle behaviour. The IMU is one of the most important components of the control system.

IMUs are usually composed by accelerometers, gyroscopes and compasses, yet other sensors and combinations are possible. The most common alternative to this design are the thermopiles. They are based on infra-red (IR) sensors that measure the temperature gradient between the sky and the surface of the earth, to then estimate the UAV attitude. This approach is widely spread among the amateur RC hobbyists and low-cost control systems. But this inexpensive approach has some drawbacks when compared with IMUs: they are less effective in certain weather conditions, such as snow, fog and rain. IMUs on the other side can operate in any weather conditions, are very accurate, but exhibit a relatively expensive price and are harder to program.

Although the platform for this UAV does not require very accurate attitude estimation, the IMU design was still preferred, due to their higher reliability that allows future UAV platforms and configurations.

It is intended to reach the maximum possible accuracy with this design using relatively inexpensive MEMS sensors, so the IMU was designed to include a 3-axis accelerometer, 2-axis gyroscope and 2-axis compass.

Accelerometer

The principle of operation of the IMU involves continuous sensing of accelerations in each of the three directional axes and integrating over time to derive velocity and position.

Companies like Sparkfun^{TM} provide a wide range of COTS solutions at a reasonable price. These solutions are often a good choice for small projects, where soldering tiny surface-mount technology (SMT) electronic devices can become a quite daunting task, because they require high dexterity and specific soldering equipment. This also grants quicker developing times, since these solutions come packed all with the auxiliary circuit.

The LIS302DL MEMS motion sensor, from ST, depicted in figure 4.1 was chosen. This low-cost and low power consumption three axes linear accelerometer is able to provide a measured acceleration through I^2C (Inter-Integrated Circuit) serial interface and has dynamically selectable full-scale from $\pm 2g$ to $\pm 8g$. It also incorporates vibration cancellation systems, through internal high-pass filters, that can be externally customized.

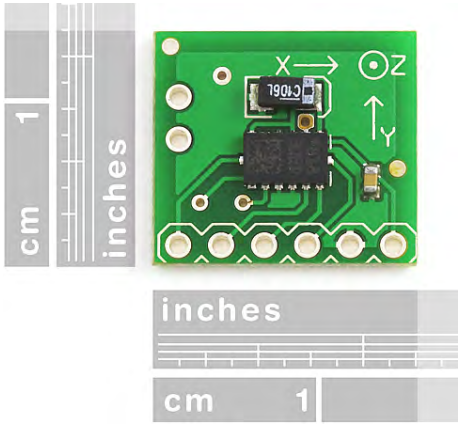

Figure 4.1: Three axis accelerometer sensor board.

The information passed through the I^2C by the accelerometer is packed in an 8-bit wide message, for each axis measurement. With this message size and with the narrowest measuring amplitude ($\pm 2g$), the maximum resolution is 15.6 mg.

The acceleration data can also be used to detect small position deviations induced by the wind. These movements are too short for the Geo-localization system be able to detect, since GPS modules have a maximum accuracy of 5 meters.

Gyroscope

For a long time Gyroscopes have been used in robots to augment the attitude perception of mobile robots [11]. But only in recent years, due to the solid-state MEMS, has this technology become practical for UAVs and other small robots. MEMS allowed smaller and cheaper gyroscopes.

It was decided to develop the gyroscopic sensor to implement in this project. Solutions such as COTS were too expensive for the bundles provided. The gyroscope is based on the LPY5150AL sensor from ST; this sensor is capable of measuring angular rate along pitch and yaw axes, and has a full scale of $\pm 1500^{\circ}.s^{-1}$.

4.1.2 Compass heading system

The robot heading is one of the input parameters for the path planning, and the actual heading is extremely important in solving the real world navigation needs of an autonomous platform [11]. The heading could be estimated through by the differential of the position data, using the geo-localization information, but the most common and reliable way is to measure the absolute heading with a geomagnetic compass. Geomagnetic sensors are one particular type of magnetometers specifically designed to sense the earth magnetic field.

The earth's magnetic field can be represented as a dipole tilted 11 degrees to the planet's axis of rotation. It is measured in Gauss, representing the magnetic flux density. The strength of the magnetic field is not static and fluctuates around 0.5 and 0.6 Gauss. Earth's magnetic field direction can be represented by the scheme of figure 4.2, represented in the UAV coordinate system.

In this figure, we can see that the earth's field points down and roughly toward north (in the northern hemisphere). The angle of the magnetic field to the surface of the earth is called the inclination angle and the angle formed by the geographic and the magnetic north is known as declination angle [13].

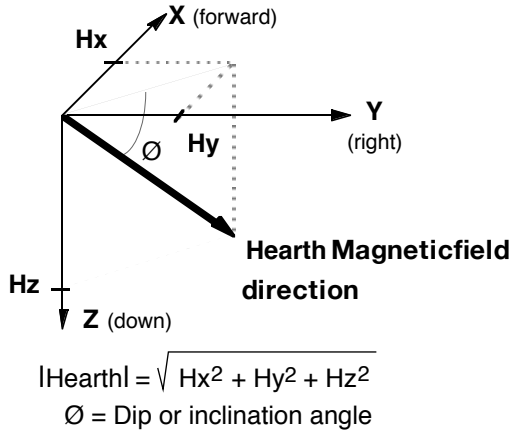

Figure 4.2: Earth's magnetic field decomposed in the X, Y and Z coordinates of the robot [13].

There are various ways of measuring the earth's magnetic field, with different types of magnetometers – mechanical, fluxgate, hall-effect and magnetoresistive based compasses. A magnetoresistive (MR) sensor selected. This type of magnetic sensor was chosen among other types due to its ability to take precise measurements at very high sample rates, low power consumption, small package size and low cost. MR sensors are best suited for electronic compasses since their range of sensitivity is centred within the earth's field [14]. These MR sensors allow reliable magnetic readings in moving vehicles at rates up to 1,000 times a second [13].

We chose the HMC1052L sensor, shown in figure 4.3, which is produced by Honeywell and is capable of measuring a magnetic field with a resolution of $120\mu gauss$. This sensor outputs the magnetic field intensity in two orthogonal directions, with a resolution of $1.0mV/V/OE$ and a measure range of $\pm 6OE$[1]. This sensor will provide the magnitude of the earth magnetic field readings in the directions of measure.

The compass will be developed within the microcontroller: this function will be capable of providing the relative direction of the earth's magnetic field, and thus the absolute heading direction of the robot from the information provided by the sensor.

Only the X and Y components of the earth's field are used when determining the azimuth. This approach, assumes that the MR sensor is always parallel to the surface of the earth, corrections have to be made if the robot is tilted. This tilt perception and

[1]Oersted (OE) is a unit, from CGS system, to quantify the magnetic field intensity.

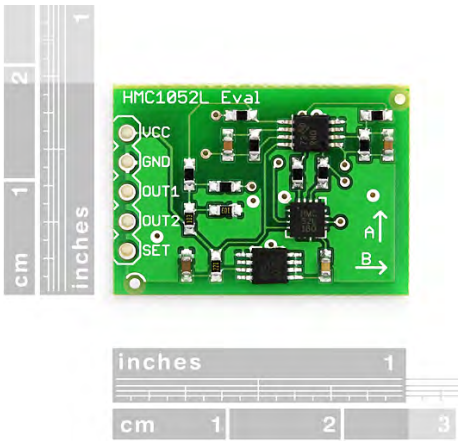

Figure 4.3: Magnetic sensor board, used to provide azimuth.

compensation can be made using the on-board accelerometer if necessary, but the blimp dynamics and natural stabilization may dismiss this compensation. Three axis magnetometers with tilt compensations were too expensive, and outfitted the requirements of this project.

The earth's magnetic field is often distorted nearby power lines or ferrous materials. This is most critical in indoor applications, and often difficults the implementation of geomagnetic sensors .

Initial tests revealed a poor sensitivity of the magnetic heading compass. This was caused mainly due to conjugation of the lower resolution of the ADC module built-in the microcontroller and the weaker strength of the earth magnetic field compared to the measuring range – earth magnetic field readings range between $\pm 0.6 OE$ and the sensor measure range is $\pm 6 OE$. This induced a low sensitivity compass system. To overcome this problem it was decided to use two INA128 instrumentation amplifiers, as differential amplifiers. To take advantage of the whole analog range and to avoid the amplifier's saturation we set a differential gain of 9, imposing an external gain resistor of 6.25 kΩ (expressions 4.1 and 4.2):

$$G = 1 + \frac{50k\Omega}{R_G} \tag{4.1}$$

$$R_G = \frac{50k}{8} = 6.25k\Omega \tag{4.2}$$

The nearest standard value 6.2 kΩ was used. The voltage reference for the differencing amplification will be set to 1.35 V, using a voltage divider composed by a 10 kΩ and a 6.9 kΩ resistors, connected to the 3.3 V and 0 V respectively.

With this design we can have the magnetic field variation spread by the whole analog band (0-3.3 V). Augmenting the compass sensitivity to 2.475 $mV.OE^{-1}$.

4.1.3 Geo-localization system

The absolute localization of the UAV is provided by the Global Positioning System (GPS).

The receiver selected was the EM-406A, seen in figure 4.4, which is manufactured by USGlobalSat and is based on the SiRF Star III chipset. This GPS module, similarly to

other commercial GPS solutions, provides limited accuracy data that is used mainly to measure the position coordinates of the UAV (x,y,z) and enable way-point and position hold manoeuvres. However the GPS output data also includes precise date and time information, course and speed over ground and other additional information regarding the solution's accuracy.

This GPS system has a positional accuracy of 10 meters, 5 meters with the wide area augmentation system (WAAS). Some advantages are the small footprint (30mm x 30mm x 10.5mm) with built-in antenna, low power consumption (70mA at 5 volt) and TTL level output voltage (2.85 V).

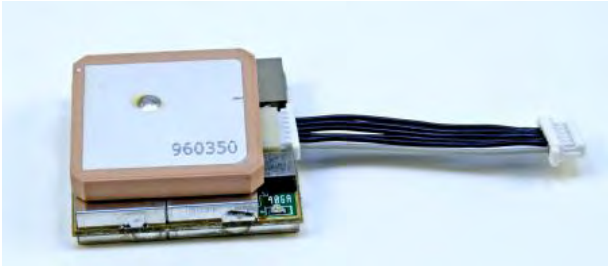

Figure 4.4: EM-406A geo-localization module.

The data outputted through the TTL serial line is formatted according to the National Marine Electronics Association (NMEA) messages. These messages are referred to as the NMEA 0183 protocol.

4.1.4 Object detection

In some applications that need a very accurate relative position of the UAV in respect to objects, as a close proximity flight, the system can not rely on inertial navigation systems or geo-localization systems [39]. Inspection and surveillance missions can very likely put the robot in these situations, requiring the ability to navigate through obstacles. Therefore, the need of system more reliable than the used by others projects was noticed. In these projects there is a pilot in permanent awareness. Moreover, this approach limits the flight perimeter of the UAV to the visual line-of-sight of the pilot.

The UAV was equipped with an active object detection system that is able to sense the obstacles clearance and activate emergency states, if necessary.

The object detection system is composed by three sonar range finders – LV-MaxSonar®-EZ0™ – from Maxbotix. These sensors are capable of detecting and measuring objects from 15.2 cm up to 6.4 meters, with 2.5 cm of resolution. These are fully assembled sonar sensors (figure 4.5) that have all the electronics needed for sonar ranging and signal processing, and three output methods are available: analog, pulse width modulation, and serial communication (where the data of multiple sensors can be transmitted in only one signal line). These low-cost sensors do not have temperature or humidity compensation,; instead, the sensor calibrates itself during each first read cycle, during which it is important to keep a minimum distance of at least 35 cm. If conditions change during the operation, the sensor may require a reboot for recalibration.

Three of these ultrasonic sensors will be used to enable object avoidance, and to allow a controlled flight close to buildings. It is crucial to have distance readings on each side

Figure 4.5: Maxbotix Sonar, with the external dimensions.

of the UAV and on the heading direction. In indoor operations an additional sonar sensor may also be required to check the ceiling clearance.

High rate and resolution altitude information at close range is also mandatory to allow low altitude flight and docking manoeuvres – the GPS only outputs altitude, which is different from the actual ground distance provided by the sonar altimeter.

Two sonars were placed faced to each side of the UAV. The third range finder will be faced frontwards, with the ability to tilt and also make ground distance measures – this solution enables a simpler and lighter control hardware design.This sonar altimeter provides high rate and resolution altitude information at close range. Figure 4.6 depicts the UAV view angles, most of the objects are detected in the central 36 degree zone – the beam width of these sensors is variable, and is actively adjusted by the sonar system software.

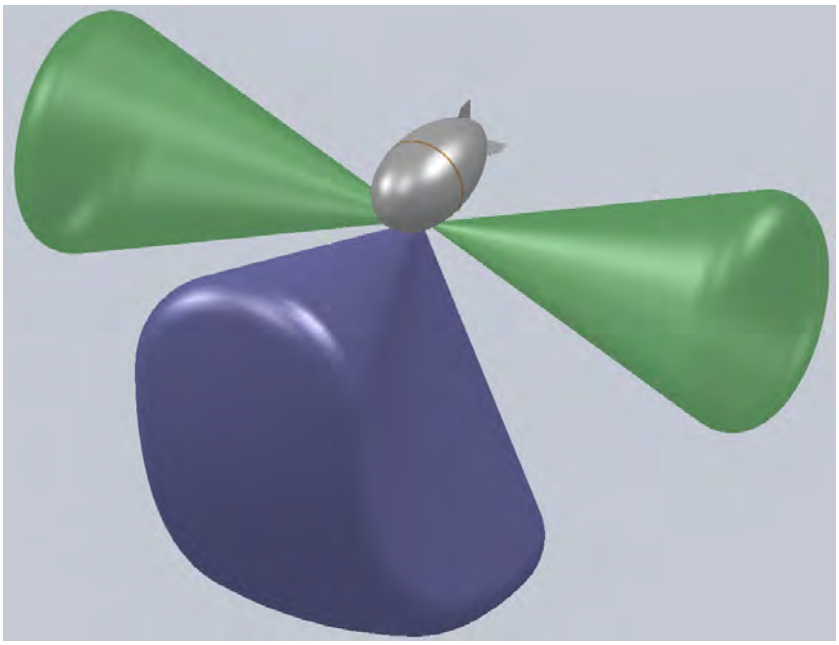

Figure 4.6: Trimetric view of the UAV and the respective detection areas.

4.1.5 Wind sensing

As discussed in section 3.5.4, the platform is very susceptible to wind gusts. In order to implement an algorithm that can handle and correct these effects, a way to sense and measure the wind is needed.

The wind relative direction is a crucial input to this system. It deeply affects the UAV's behaviour and position.

The wind relative airspeed can be determined merging information given by other sensors. Knowing the UAV's nonlinear dynamic model and the speed relative to the ground, the relative airspeed can be estimated, this processes is further discussed in section 5.1.3, page 57.

With the relative wind direction, the trajectory planning can be programmed to give certain directions to the blimp that attenuate the wind effect. When the blimp is faced towards the wind, it is able to withstand stronger winds and correct position deviations more efficiently – figure 4.7 demonstrates one example of the implementation of these planning techniques. With the current platform it is impossible to follow this flight path accurately, since is not possible to move the blimp sideways. This example demonstrates the theoretical application of a path planning, considering the wind relative direction variable.

The wind relative direction information can be vital to the system path planning, witch enable the UAV to keep the reference position and trajectory, even with high wind speeds.

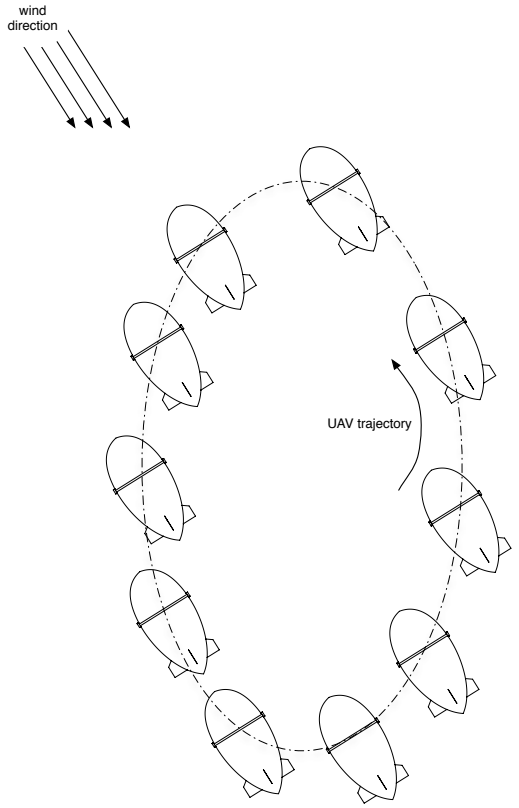

Figure 4.7: One ideal example of the wind effect on the path planning, were the UAV is always heading to the wind.

Wind direction measurement systems, are widely used in sail ships and weather stations, these sensors are designed to withstand adverse conditions, they are robust and subsequently large and heavy. No commercial solutions are available to be implemented in UAV platforms. Other academics projects developed their own wind sensing sensors [21, 18], yet, these solutions are designed to fit in large LTA platforms, and are too heavy to be used in the UAV developed in this thesis.

So was decided to custom design the wind sensing system. To measure the relative wind direction an 8-bit absolute encoder was used. This cost-effective encoder (figure 4.8) weights only approximately 14 grams. The rotational torque needed to turn the encoder is 0.5 $N.cm$, and it outputs the information through a Gray code.

Figure 4.8: Bourns absolute encoder, with 8-bit resolution.

Was attached a flat plate to the rotational shaft of this encoder. The flat plate and its distance to the rotational center must be adequately designed to ensure that the encoder orients itself even with a slightly breeze. The moment created by the wind is determined according to the expression 4.3, where F is the composition of the lift and drag forces produced by the flat plate and is given by the expression 4.4.

$$M = d \times F \tag{4.3}$$

$$F = L.\cos(\theta) + D.\sin(\theta) \tag{4.4}$$

where L denotes the lift force produced and D the respective inducted drag; θ denotes the angle formed between the wind and the encoder axis.

On the digram of the figure 4.9 it is possible to identify visually the forces acting on the encoder flat plate. Note that the lift is always perpendicular to the air stream and the drag collinear.

The lift (C_L) and drag (C_D) coefficients are related to the angle of attack (θ), this dependency is stated on the polar plot of the respective airfoil. The C_L and C_D enable the determination of the total lift and drag produced by the airfoil, in this case a flat plate. This flat plate airfoil is the extreme case of the thin symmetrical airfoil theory [23, 4], in which is stated that the lift coefficient of an infinite wingspan airfoil is directly related to the angle of attack in radians (expression 4.5):

$$C_L = 2\pi\alpha \tag{4.5}$$

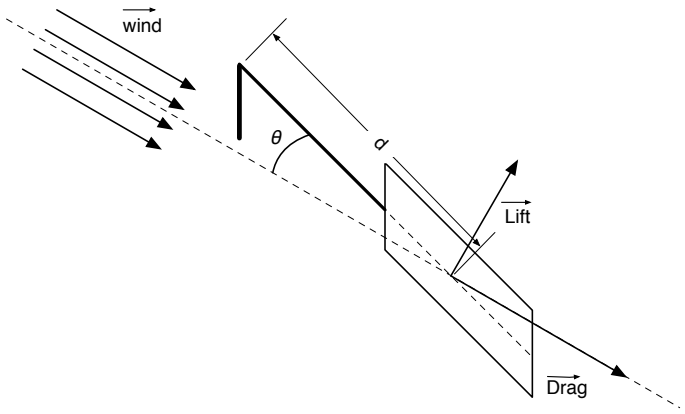

Figure 4.9: Wind relative direction measurement diagram.

A precise determination of the area needed orient the encoder for the total range of attack angles would lead to extensive calculations. These formula is only valid for angles of attack up to 15°, for larger values the flow is too turbulent and the drag grows rapidly.

To design the flap plate area, the performance of a flat plate at a 15° angle was analysed. Neglecting the drag contribution, and then applying a factor of safety (FOS) over the area of the flat plate, in this conditions and by equation 4.5, results the corresponding C_L of 1.64.

The area can be then determined according to the expression 3.14, on page 30. Where the C_D is replaced by C_L, and the dependent variable is the area. Establishing the length at 10 cm for the first iteration, result a lift force, needed to overcome the shaft torque, of 0.05 N. Then the area, for a heading wing of 1.5 m.s^{-1}, will be determined from the expression 4.6.

$$\begin{aligned} A &= \frac{2 \times Lift}{\rho \times v^2 \times C_L} \\ A &= 0.022m^2 \end{aligned} \tag{4.6}$$

From the first iteration resulted an impractical large area, 0.022 m^2. Therefore, the arm length was extended to 25 cm, the lift force needed is only half of the initial and the area is:

$$A = 0.009m^2 \tag{4.7}$$

An aluminium sheet of 7 by 13 centimetres will enable wind direction readings. On figure 4.10 is shown the encoder and all the parts that compose the relative direction wind measurement sensor. Is important to keep in mind that for small angles the lift produced decreases and it is possible to have an error of 1 to 4°.

4.1.6 Visual imaging system

Visual sensing can provide a tremendous amount of information about the surrounding environment, and it is potentially the most powerful source of information among all the sensors used on robots [11]. Still, due to the amount and the complexity of information,

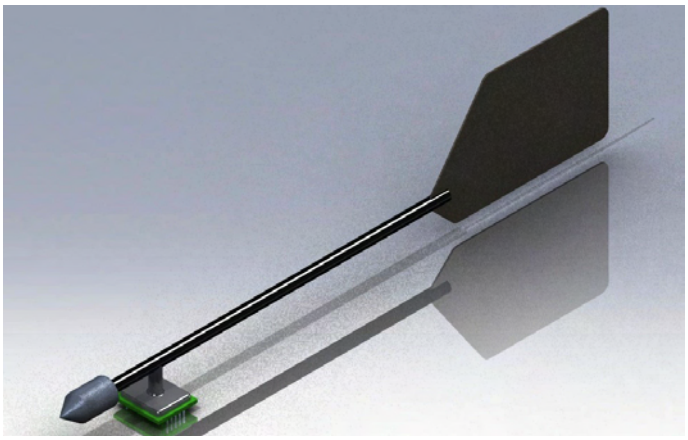

Figure 4.10: Wind relative direction measurement system.

extracting visual features for positioning and navigation is not an easy task. On-board image processing systems demand high processing times and capabilities, making these systems heavy and high power demanding. LTA platforms that rely on vision-based algorithms are very large, usually having more than ten meters long.

With the control architecture implemented, the image acquisition system works separately from the embedded control system. The images are directly sent to the base station through proprietary wireless communication. The ground station computer will then acquire the video and present it to the operator through the GUI.

Nevertheless, vision-based algorithms may be implemented in the ground station. With this design, image based reaction times may be longer, but this information is not time-critical to the UAV's security and mission success.

The image acquisition system is based on a small wireless security camera, shown in figure 4.11. This camera captures color images at a 30 frames per second. The images are transmitted to the ground station through an embedded 1.2 GHz data link.

On the base station one analog-to-digital converter is needed to convert the RCA signals to digital information, which can be used in the GUI or for visual algorithms.

Figure 4.11: Wireless security camera system.

To increase the camera utility it was mounted in a tilting servo, which enables acquiring videos such as bird-eye-view over ground, as well as capturing images on the heading direction.

It is intend to manually control the servo from the ground station, but the control system can take control over the servo. Since the ultrasonic range finder is attached to the same tilting structure, the control system may need to specifically orient the servo, for example in landing manoeuvres, where high rate altitude measurements are needed.

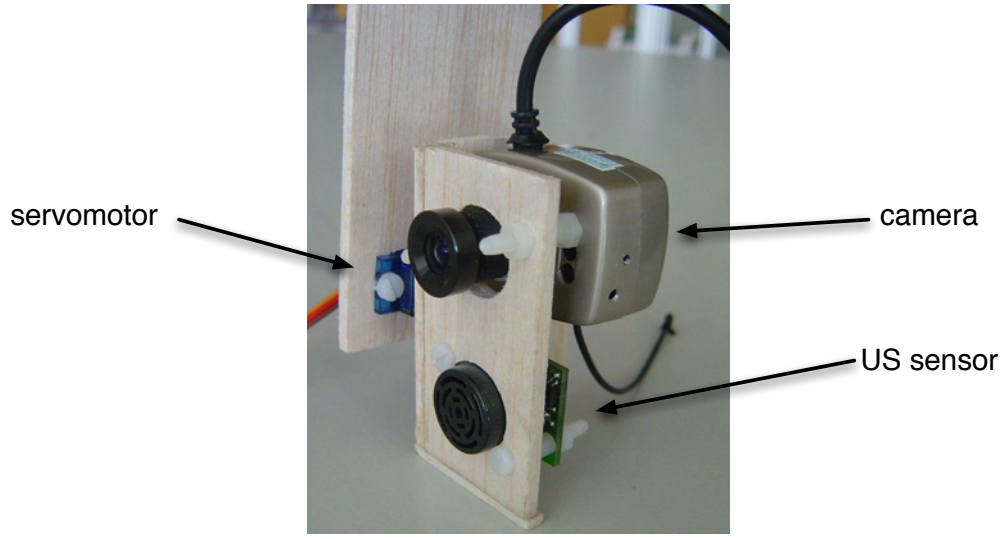

Figure 4.12: Tilting camera system mounted on a light structure.

4.2 Real-time wireless telemetry

The wireless data link is granted by two XBee Pro embedded RF modules (figure 4.13), manufactured by Digi™, they are based on ZigBee mesh networks. They are also well known for their COTS serial universal asynchronous receiver/transmitter (UART) interface, that can act as a wireless "serial line replacement".

These modules have a built-in microcontroller unit (MCU), which implements all of the wireless protocol stack, and also enables other unique features, such as, digital I/O data passing, analog data passing – through analog-to-digital converter (ADC) and pulse-width modulation (PWM) outputs. These features, and other operation characteristics, can be programmed in run-time through AT commands, or by the application programming interface (API) provided by Digi.

The modules provide outdoor RF communications up to a maximum distance of 1.6 km, and indoor communications within a 90 meter range, with a serial interface data rate of 115.000 bps.

These modules will be used to enable real-time wireless telemetry between the robot and the ground station, while sending and updating the mission objectives.

The ability to send hardware interrupts from the ground station will be also integrated and there will be three hardware interrupts that may be used to activate emergency states,

Figure 4.13: XBee RF module used.

activate or deactivate hardware functions and other convenient interrupts, as discussed further in chapter 5.

A printed circuit board (PCB) was designed to use in the ground station and enable the communication with the computer. This board converts the TTL voltage level serial data to serial RS-232 voltage compliant signal. On the upper right corner of the board (figure 4.14) are presented the 3 tactile switches to send hardware interrupts to the robot.

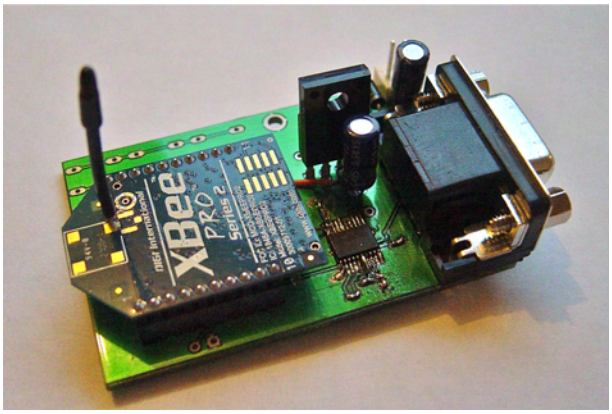

Figure 4.14: Custom designed PCB to connect the XBee module to a computer.

4.3 Control board

Most of the research and development UAV projects rely on large platforms to achieve a high level of autonomy and intelligence. This thesis takes a novel approach: we intend to develop a platform capable of conducting reconnaissance and surveillance missions either in indoors, in constrained areas or outdoors, which are missions that generally preclude the implementation of those types of vehicles. This goal limits the blimp dimensions and consequently its processing capabilities. This trade-off was discussed with more detail in section 3.2.1.

This thesis aims also at developing a UAV based on limited hardware control capabilities. Therefore it is necessary that the heavier processor tasks are made by the ground

station, transmitting back the subsequent results to the UAV. A good example of such tasks are the image processing algorithms and the complex path planning trajectories generation.

The embedded control board and all the sub-systems developed for this platform need to be as light as possible. This also includes lowering the power consumption to the minimum.

The embedded control board developed has all the electronic systems needed for signal processing and acquisition, and to control the UAV.

4.3.1 Architecture overview

The system architecture was designed to implement the objectives defined for the project. A function diagram was made to structure and express the ideas and objectives to incorporate in the UAS (figure 4.15). The diagram depicts the interaction of different systems.

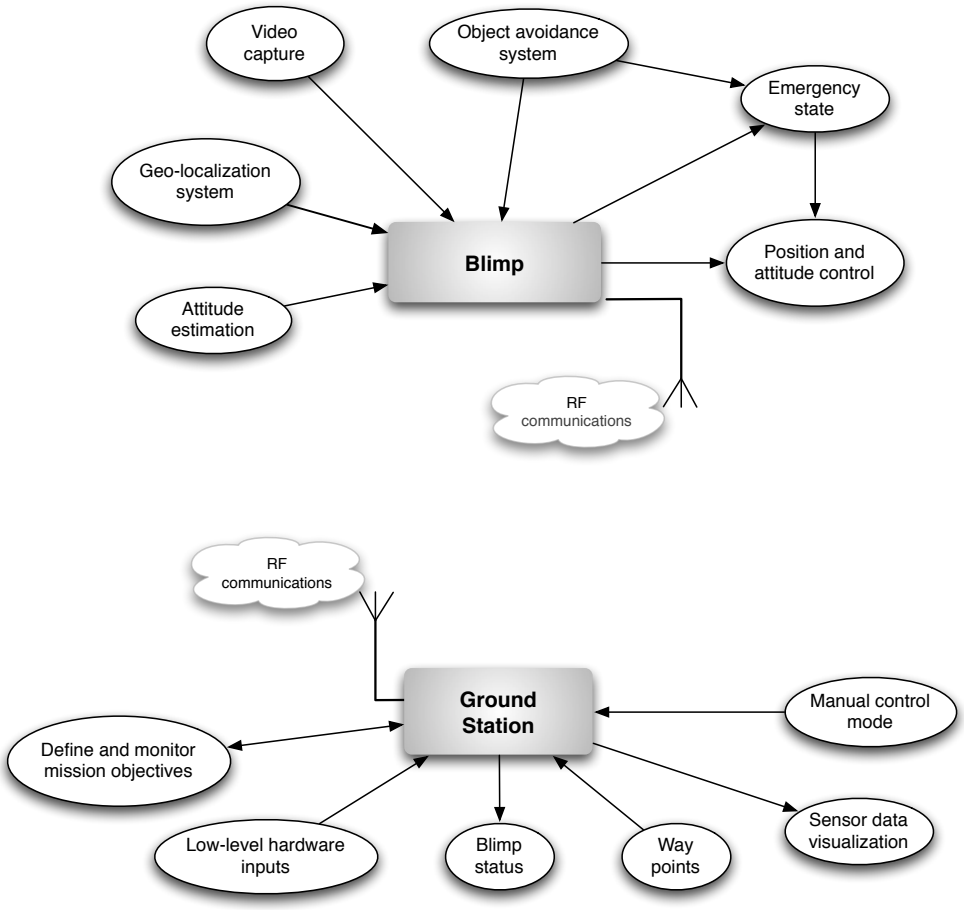

Figure 4.15: UAS' functions diagram.

All data acquisition and processing is made by two MCU from Microchip running at 3.3 Volt. The two MCU architecture system has the objective to make the control system more reliable and independent of the platform. Moreover, a solderless socket for the

highest level MCU endows the platform with more flexibility. Enabling future upgrades to the microcontroller. Two 16-bit PIC from the PIC24F and PIC24H family were chosen. The PIC24FJ48GA002 and the PIC24HJ128GP502. The latter MCU is more powerful and has also more memory. These two PIC working simultaneously grant an on-board processing power of 56 MIPS.

The PIC24F MCU is responsible for the low-level algorithm, controlling the three motors, determining the best vectoring angle. This MCU also controls the camera tilting servo and measures the path clearance. The thrusters are controlled by three H-Bridge integrated circuits (IC) that are able to control brushed DC motors with a maximum continuous current of 5A at a maximum voltage of 28V.

The PIC24H MCU deals with the high-level path planning and pose estimation algorithms. This MCU is also responsible for data packaging and sending to the ground station. The PIC24H has roughly threes times the processing capacity, 40 MIPS against 16 MIPS of the PIC24F.

There is no long-term data storage system in the control board. All the information is sent to the ground station. That has the ability to store the telemetry information regarding the vehicle pose and other mission characteristics over time.

The board hardware architecture, with the organization of all the sensors discussed in this chapter, is demonstrated in the diagram of figure 4.16. This diagram evolved from the functions diagram of figure 4.15. This diagram depicts the architecture of the complete UAS, including the systems developed for the ground station.

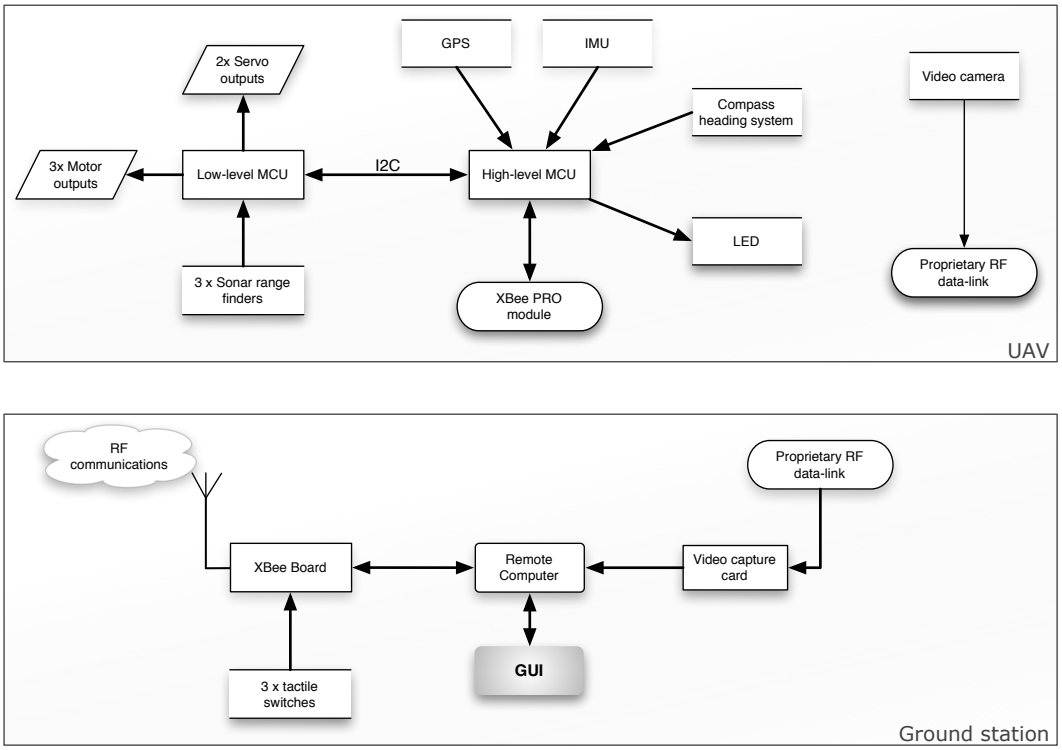

Figure 4.16: Technical diagram of the UAS' integrated systems.

All the electric components and motors are powered by the board. The voltage that

supplies the motors is unregulated, and the motors loads are controlled using PWM signals. The embedded power supply regulates the voltage to 5V and 3.3V to power the electronic systems.

All the sensors and electronics were incorporated in an 80 by 127 millimetres board. When available, we opted for surface mounting components, which will enable space savings. Both the H-Bridges and the lowest level PIC are in small-outline integrated circuit (SOIC) package standards. The control board developed is depicted in figure 4.17

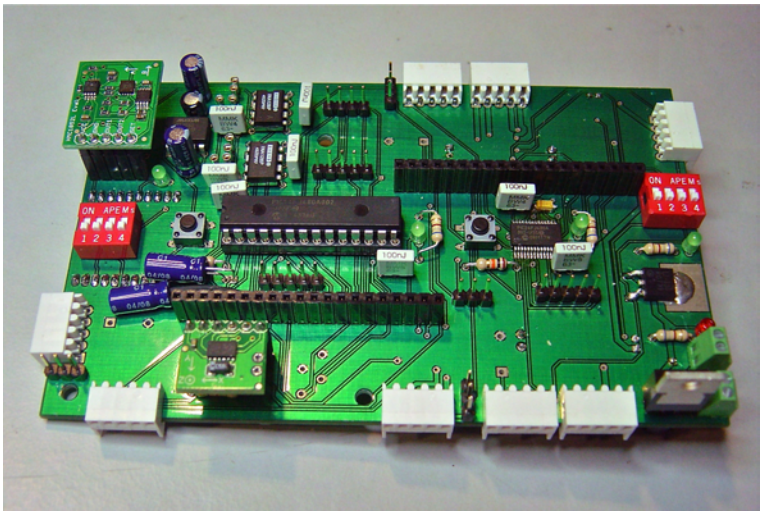

Figure 4.17: Embedded control system.

4.3.2 Additional features

As a parallel objective, it was stated the need to develop an embedded control board that may be used in a wide range of platforms, airborne or not. With the two microcontroller architecture, it is possible to keep the same high-level algorithm, and adapt the low-level, hardware oriented control, to the specific platform. The low-level control will then generate the appropriate outputs according to each platform.

The H-bridges can be used to drive 3 independent motors, and the 3 servo outputs may be used to steer the vehicle, or to control more motors, with RC motor drivers that are controlled with PWM servo signals.

This control board may be easily adapted to control hovercrafts, boats, wheeled vehicles, fixed-wing aircrafts and other platforms similar to helicopters.

All the MCU from the 16-bit Harvard architecture are pin compatible to each other, therefore they can be switched without having to modify the connections. Moreover, these PICs have the remappable pins function. These characteristics ensure that this board will operate correctly with other MCUs if more processing capabilities are needed.

Another feature of this control system is the integration of a high-power LED. This LED may function as a warning visual signal, or be used to illuminate the UAV during night missions. The LED will be placed on top of the linking belt, faced down, to created its visibility from the ground. Figure 4.18 demonstrates the surface mounting LED and the

respective board designed.

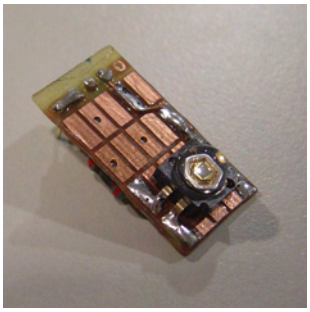

Figure 4.18: An image of the LED board designed.

The images 4.19a and 4.19b depict the embedded control system mounted on the aerial platform and the orientable camera and sonar system.

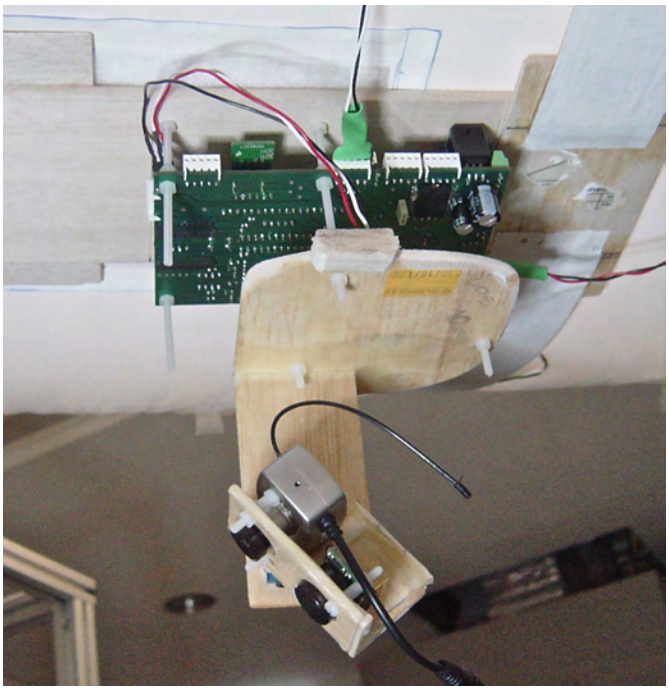

(a) Side view of the assembled control board, camera and sonar.

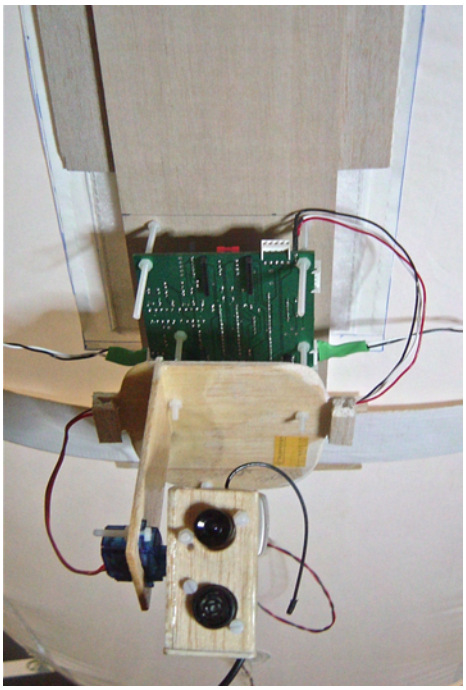

(b) Frontal view of the control system.

Figure 4.19: Different perspectives of the on-board control system mounted on the robot.

Chapter 5

Sensors and actuators interface and communications

The typical target missions of unmanned aerial vehicles are surveillance and reconnaissance, infrastructure inspection and environmental monitoring missions.

As the possible applications field for UAVs grow significantly, higher levels of autonomy and less complex systems are demand. Present solutions require a large crew of operators to control the vehicle and manage the mission objectives.

Managing and control an autonomous air vehicle in a partially known and uncontrolled environment is a complex problem, especially when the mission takes place in an environment with many threats or even when the UAV needs to fly in constrained areas.

The control algorithm has to deal with all these situations that threat the UAV integrity and the security of people in the ground, plus the mission objectives management. In this thesis, the challenge is even bigger because the control is to be made by a limited capacity embedded control system.

For the robot being developed, a high level of autonomy is required in order to make the robot more independent of continuous communications with the ground station. It must also retain the ability, if the operator demands it, to be flown directly (manual mode). This will be achieved applying a two layer logical hierarchy of control.

The highest level of control will deal with mission planning, trajectory generation algorithms, vehicle waypoint navigation routines and establishing communications with the control center.

The lowest level will be responsible for actuating the servos, motors and other control outputs. It will accept inputs also from the upper level. Low-level sensors such as distance measurement sensors are intended to directly activate emergency states in this level. These emergency states can be used to prevent collisions and safeguard the UAV integrity in the event of component failure, extreme operating conditions or external disturbances.

This chapter addresses the algorithm and the development of the communications protocol. Firstly, the algorithm needed to process the sensors information is developed, as well as the algorithms used to control the UAV and the communications protocol.

Afterwards, the software to implement in the ground station will be developed. That includes the graphical user interface application, and the XBee modules programming settings.

5.1 Data acquisition and processing

This section describes the algorithm developed to process the raw information provided by the sensors, which ultimately indicate the vehicle pose.

5.1.1 Accelerometer

The LIS302DL accelerometer outputs the information through the I^2C serial line. The I^2C protocol allows the connection of up to 112 devices (with the standard 7-bit addressing) using only a two-wire synchronous serial interface. The LIS302DL works natively with the I^2C standard mode with frequency clocks up to 100 kHz, but it is also compliant with the fast mode that enables clocks up to 400 kHz.

To avoid multiple addresses in the the same line, this accelerometer has two possible addresses. The address selection is made by an input pin, which controls the least significant bit value. The address used was `0011100x`, where the least significant bit indicates the read or write command, the seven most significant bits are the device address.

Values read on each of the three axis are stored in three local registers, that can be read using the I^2C interface. The content stored in this registers are represented using the 2's complement system.

The data is read by sending the read command to the slave device; after receiving the acknowledge of this message, the register address to be read is sent. This procedure may be executed at an 100 Hz to 400 Hz rate.

After the interpretation of the data in the 2's complement form, its integer equivalent is stored in the respective variable.

5.1.2 Compass heading system

From the two axis field intensity readings is possible to extract the UAV heading direction. The two values are function of heading angle, namely, yaw. The field intensity in UAV longitudinal axis is described by $B.cos(\psi)$ and on its orthogonal axis is described by $B.sin(\psi)$, where B denotes the field intensity. The UAV heading direction can be determined from the arctangent of the quotient of the division of the two readings [15](expression 5.1):

$$\psi = \arctan\left(\frac{B_Y}{B_X}\right) \tag{5.1}$$

where, B_Y and B_X denote the field intensity in the y and x axis of the UAV, respectively.

In C programming language the function that computes the arctangent is the `atan2(y,x)`. To avoid the arctangent function undefinitions, special cases were included in the code.

The magnetoresistive sensor used outputs the readings through analog voltage. When no magnetic field is sensed the voltage is $\frac{V_{cc}}{2}$. The outputted voltage is, then, lower when the field flux density is negative and higher when the field is positive.

Offsets from the center value are imposed by nearby ferrous objects and by the control board itself.

To obtain symmetrical axis readings, oscillating around the 0 OE reference, a software offset value must be inserted.

5.1.3 Geo-localization information

The GPS module provides the absolute three dimensional coordinates of the UAV. This GPS module has 1 Hz update frequency; this means that on each second a new solution is outputted from the GPS. The data sent at 4800 baud, through the TTL-level serial line, follows the NMEA 0183 standard.

The six different sentences sent each second by the GPS (GGA, GSA, GSV, RMC, VTG and GLL) contain a large amount of information regarding the solution and the associated accuracy. They provide, also, other useful information such as date, UTC (Universal Time, Coordinated) time, and a checksum value [47]. The NMEA sentences do not exhibit a fixed length format, but each sentence type has a fixed number of fields. Even if no information is available to be sent, the reserved space is sent empty.

The GPS altitude information is more accurate than the one associated with the horizontal plane coordinates. When paired with the ground clearance, measured in the initial phase of the flight, by the tilting sonar, the GPS can provide timely information of altitude and, more important, the ground clearance.

The *speed over ground* field present in the VTG sentence, contains the information of the velocity of the UAV over ground. This information, connected with the thrusters load and the blimp dynamics model, allows the relative air speed to be determined. This sentence provides also information of the *course over ground* that gives an estimate of the heading direction based on previous GPS positions. This information can be used to minimize the error the compass heading system.

After the sentence reception and identification, the string is split into sections. The desired information is then converted from string characters to integers, booleans or doubles variables types, and the information is directly stored in the respective variables.

GPS alone can provide a good source for outdoors navigation, specially to higher altitudes UAV where the obstacles are not a issue. Yet, GPS based navigation is restricted to open space mission. The GPS signals are affected by near tall buildings and high density urbanized areas. In these cases, other navigation techniques must be developed.

5.1.4 Position estimation

An accurate position estimation does not depend on one sensor information only, but rather on an array of sensors. The sensors information is then merged to give an estimation of the vehicle attitude; this can be achieved using a Kalman filter [10].

Typically Kalman filtering techniques are applied for position estimation, the reliability and accuracy of these systems depend on the position measurement technology applied. However, the autonomous control of helicopters and other VTOL platforms with different control modes is more complex and motivated the research activities of several universities [39].

According to the actual UAV position and the next desired position, the control system determines the variation of the position and attitude, it also computes, a velocity indicator. The subsequent information is then sent to the lower level control hierarchy, which is responsible to manage the hardware to accomplish that objective.

5.2 Higher-level control hierarchy

The higher level algorithm layer is responsible for the position estimation, and it is where all the decisions that affect the vehicle state are made. But the higher level control hierarchy is not only responsible for the position and attitude control. In this level are implemented other functions that monitor the MCU functioning such as fail-safe states, communications management and the UAV mission objectives and payload management.

The algorithm is based on a main loop that cyclically checks for new sensor data and then determines if any action needs to be made. Whenever a new reading is made the corresponding flag is activated, indicating to the main loop that a new reading is available. The reading and reception of information are all started and accomplished with CPU interrupts.

5.2.1 Active security systems

A function to check if the code is still running properly was implemented. This was achieved using the watchdog timer (WDT) embedded on the PIC. If one of the MCU stops running properly, the WDT overflows forces the respective microcontroller to reset.

Additionally a fail-safe state was included. This state is intended to keep the UAV integrity upon a code failure, or is some conditions are exceed. This emergency state can be also remotely set, or re-set, by the user through the graphical interface or by directly pressing one tactile switch on the xbee board.

While in this state the thrusters are set to their highest load, the vectoring angle set to -90 º (downwards position) and the LED blinks. This is made to make the UAV land as fast as possible, and at same time send a warning signal for the ground – to ensure that one gets injured by the descending blimp.

5.2.2 Manual mode

If the user spots a possible threat to the UAV security, or if the UAV pilot system is not capable of manoeuvring the UAV through the desired path, the embedded control system can be switched-off. The UAV is then directly controlled by the user through the GUI implemented. This command sent by the monitoring application generates a software interrupt on the MCU.

In the manual mode the blimp is controlled only through commands sent by the ground station. While in this state the necessity of timely communications accrues. The commands used to control the UAV are addressed in section 5.4.

5.2.3 I^2C communication management

The I^2C bus is a two-wire, the SDA (serial data line) and SCL (serial clock line), serial interface. On a single I^2C bus can be connected up to 112 slave devices and one master device. The master is responsible for generating the clock signal. It is the master device that always starts the communication and it first transmits the address of the destination device.

The I^2C bus protocol is very straightforward to understand, but its implementation has not benn so easy, as the UART communications, for example. Since the protocol is not embedded in the microcontroller, we have to develop functions to implement the I^2C bus protocol.

Already connected to the I^2C bus are the two microcontrollers (one as master device) and the accelerometer. This protocol is a great way to add sensors and/or data loggers to the control board. An additional socket was included in the board to easily accommodate other I^2C devices.

The communication between the two levels of control is more complex than the one needed to read the accelerations readings. Mainly due the larger amount of information exchanged, a two byte communications protocol has to be implemented.

The lowest-level MCU has four embedded functions that can be controlled and monitored by the control system, under these four function categories are 17 independent devices. On table 5.1 are presented the 17 different devices connected to the low-level MCU.

Table 5.1: Functions implemented in the lower-level MCU, that can be controlled or monitored.

function	quantity	values associated	units
thrusters load	3	0-100	%
servos positioning	3	0-180	º
auxiliary I/0	8	0/1	inch
sonar range finder	3	0-255	bool

To ensure the best speed when reading and writing to these functions, a bit-level protocol was implemented. Since the resolution of the information exchanged occupies a complete byte, the addressing must be sent in a separated byte. The total number of addresses predicted are 34, that are the 17 available functions plus the read/write information.

The former byte contains the function address with the read or write indication, and the latter byte holds the information associated to that function. The value to set or read from de device is encoded as a typical 8-bit integer.

The first byte is always sent from the highest-level to the lowest-level MCU, but depending on the read or write indication the latter byte may an reply to the former one. The headers of messages exchanged between the two layer control hierarchy are stated in the table 5.2.

The four most significant bits indicate the target function, the following 3 bits address the device and the least significant bit has the read/write direction (1- read; 0- write).

Figure 5.1 depicts one message example, this message is addressed to the second thruster with write indication. In this message is sent the order to put the left thruster at 100% of its capacity.

Table 5.2: Lowest-level MCU functions and devices addresses, with the read and write bit (R).

function	address
thrusters	1000 xxx R
servos	0100 xxx R
sonars	0010 xxx R
I/O	0001 xxx R

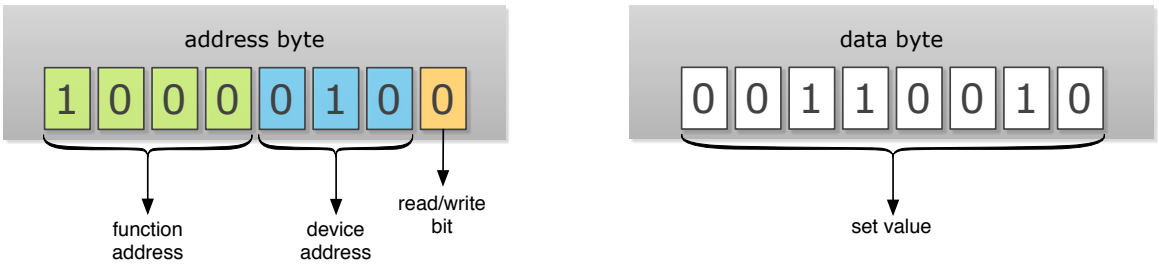

Figure 5.1: Message sent to the lowest-level MCU, to set the second (left) thruster to full throttle.

5.3 Low-level hardware oriented algorithm

The lower level MCU, according to the instructions received, controls the hardware outputs to make the UAV react correctly. The Δx, Δy, Δz and the speed indicator informations sent by the higher level path-planning, are converted to hardware outputs by the lower level code.

This hierarchy level deals also with the object avoidance and safeguard distance keeping functions. The wind sensor was also incorporated in this level. This solution is not consistent with the control hierarchy defined, but it was necessary due to the number of ports needed to read the encoder data: the higher level MCU does not have enough free ports.

5.3.1 Thrusters control algorithm

The thrusters are controlled using high frequency PWM outputs. The H-bridges used have two main inputs to control the motor rotating direction and speed; the H-bridge has more inputs but to simplify its usage they have been tied to logic high or logic low to according to their function [20]. The PWM outputs used to drive the H-bridge must be alternated between the two input ports. On table 5.3 is presented the thruster behaviour according to the input states.

The H-bridges output are computed according to the movement required, the corresponding speed an the desired UAV dynamic behaviour. The tail thruster control is preformed to achieve the yaw angle control, or y movement (in the world coordinate system) when followed by a x movement.

Table 5.3: Truth table that states the direction of thrust produced according to the inputs.

input 1	input 2	Thruster state
0	0	freewheeling low
0	1	reverse
1	0	forward
1	1	freewheeling high

Control of servomotors

The servos angular position control is made using coded PWMs outputs – this is the standard control method for RC components. The PWM frequency is fixed at 50 Hz and the pulse width duration determines the angular position: 1 ms corresponds to the 0 degree rotation the position increases linearly up to 180º, when the pulse width reaches 2 ms. The signal must be maintained in order to the servo reach and hold the desired position.

For the vectoring thrust angle we defined that the rotational reference position will be the horizontal position. Then the +90 and -90 degrees represent the upwards and downwards positions of the ducted fans, respectively.

The tilting camera and sonar rotational reference is the horizontal position too, but in this case the rotations accepted vary from 0 to 180 degrees. Were the 90 and 180 degrees represent the downwards and backwards positions, respectively.

The vectoring angle is computed from the correlation from x and z components of the movement. The function `atan2` with Δx and Δz has arguments returns the vectoring thrust angle.

5.3.2 Object detection

The lower level MCU periodically reads the sonar readings to check the obstacles and ground clearance. As soon as these clearance values reach a pre-determined threshold, a warning flag is activated and an evasive manoeuvre is started.

Based on the dynamic response of the blimp, addressed in the section 3.5, a lateral minimum clearance of 2 meters and a longitudinal clearance of 2.5 meters was established. This clearance keeping is specially critical in outdoors flights, where the conditions may change rapidly.

When flying in indoors spaces, these sensors assume another and not less important role. In these scenarios, no absolute localization system is available, so it is even more important to timely measure the walls, ground and ceiling clearance. They can provide a higher environment perception to the operator, where no other guiding systems are available.

In indoor spaces, the autonomous capabilities of the UAV are reduced, some sensors provide less accurate information, such as the compass heading system; other such as the GPS, are useless. So, it is important to keep the operator aware of the surrounding environment to best manoeuvre the UAV.

In indoor environments sonar sensors and the video camera offer the best sensing capabilities to be used as the primordial inputs for navigation.

5.3.3 Relative wind angle

The 8-bit encoder ensures a resolution of 1.4° in the relative wind direction readings. The information is sent from the encoder through a parallel interface.

The ports are sampled and their binary values stored in a single variable. Then the Gray code data is decoded, and the relative wind direction is stored.

5.4 RF communication protocol

The messages sent through the wireless data link obey to a specially designed protocol. Due to the diversity and the amount of the information to be sent, the data does not fit in a 8-bit packed message. The latitude information alone uses a 9 digit number, that may need up to 30 bits to be represented.

This solution is not as much optimized as the bit based message, but the packetization and de-codification of the messages are simpler. Moreover, the message can be visually verified, using a serial terminal emulator. To optimize the communications, and avoid serial line overflow, the message has not a fixed size; according to the information to be sent, the message is composed and sent. If no new information is available, then that field will not repeated.

A message starts always with the sender identification, then is followed by a flexible space that contains the information, and is concluded with the respective checksum. This structure was based on the NMEA sentences but in this case we adopt a flexible space sentence. In the NMEA sentences the data field is always associated with the same information, dispensing the inclusion of data headers. The NMEA design works well for structured data, but it fails if the protocol must predict future versions and be capable to accommodate new exchange information.

The messages start with the "+" character and the different messages sections are separated by the "#" delimiter, the message ends with the <CR><LF>. The information is preceded by the respective header, this header has a fixed length of 3 digits. The headers implemented are identified and described in table A.1 in appendix.

In the data section the headers and the respective value are delimited by the , character. The message itself does not have a fixed length nor a fixed number of data fields, but each data field obeys to a specific and structured data length, defined according to the information resolution.

The checksum is used to check the integrity of the message received. If it does not match with the received message, the message is discarded. The checksum is determined applying the XOR operation between all characters (until the last #), then the result converted in to hexadecimal base is attached to the message.

In figure 5.2 is presented one message example sent from the UAV to the ground station, where the individual message sections and their description is highlighted.

Messages sent by the ground station are interpreted by the robot as orders. If the previous message had been sent by the ground station to the UAV, the coordinates would

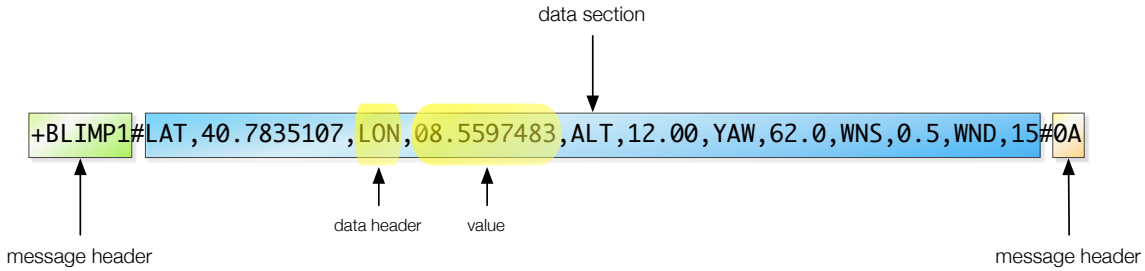

Figure 5.2: Commented message example, sent from the UAV to the ground station.

interpreted as the next destination for the UAV. On the other hand, messages sent by the UAV are interpreted as status reports.

When the manual mode is activated the operator can control the thrusters and the vectoring servo directly from the graphical interface, using for the respective commands, stated in table A.1.

XBee® modules come pre-programmed with standard 9600 baud and transparent mode operation [17]. While in this mode, the messages are broadcast to any XBee® module in range. To enable faster and secure communications and enable the I/O line passing features, the modules' parameters and firmware were tuned. Using the API provided by Digi, the modules were programmed with the following parameters:

- 32-bit source and destination address;
- 115.200 baud rate;
- encryption enabled;
- three digital I/O enabled;

5.5 Graphical User Interface

The UAV under development is intended to be controlled by only one operator. So the GUI will only present to the operator the information required to accomplish the mission and relevant data regarding the robot itself.

The robot must be capable of dealing with some the tasks by its own, leaving the operator more focused in the mission objectives. These issues were taken into account when developing the GUI and the control architecture of this project.

The program that launches the graphical interface was written in C language. The program is splited in two independent processes. The former is endowed with the communications and is responsible for decoding the information to be sent to the UAV. The latter processes is responsible for the graphical interface management. This architecture ensures that the communications will still work even if the graphic interface crashes.

The communication between the two processes is made using two shared-memories to store the information and two interrupt signals to alert the other processes whenever any new information is available.

The graphical interface was made with the GTK+ toolkit, also written in C. The GTK+ offers a great stability and performance, granted by the C source language. Moreover, this toolkit, that were initially developed to work with the X-window system, namely X-11, is now cross platform being compatible with Unix and Linux, Windows, and Mac operating systems.

After defining the message protocol and the information changed, the GUI was developed to display that information and control the UAV. Figure 5.3 depicts the interface developed.

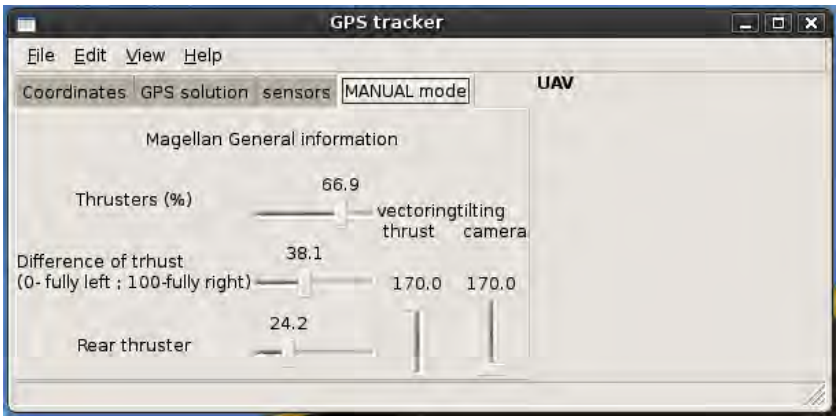

Figure 5.3: User interface developed to control and monitor the UAV.

The application developed has the ability to create and review older missions data. The UAV position and attitude over the time is recorded in a text file, using the same protocol implemented in the RF communications.

Inside the GUI is displayed a map that shows the UAV actual position and the azimuth.

Chapter 6

Results and Conclusions

This thesis does not aim to radically innovate in the LTA technologies, but rather build a concise and robust platform for future projects, and includes some novelties in the field of small lighter-than-air unmanned vehicles.

Typical lighter-than-air UAVs have lengths greater than 10m. This project was intended to develop a unmanned aerial system based on a LTA platform and using off-the-shelf low-cost sensors. This platform was based on low power requirements, and light weight MCU.

After developing the systems and techniques required to accomplish the objectives stated for this thesis to develop a platform endowed with autonomy capabilities, able to provide real-time telemetry for surveillance and monitoring missions, it is important to verify the system performance.

To validate the solutions adopted, and the UAV platform as a whole, some experiments and flight tests have be conducted. The sensors, the reliability of the wireless communications and other subsystems have to be tested, as well as the performance of the protocol developed for the information exchange between systems (local and remote).

The first tests concern the embedded control system performance and functionality. As the algorithms for the sensors were developed they were tested to validate the communication protocol used, the sensor accuracy and robustness.

The RF communications were the first system to be implemented and tested. The wireless communications were used as a debugging method for the algorithm and allowed more flexibility to test the other systems. The XBee modules provided excellent RF communications and offered a great communications range. They are reliable and the communications bandwidth is large enough for this project needs.

The ultra-sonic range finders provide a good accuracy in measuring the distance to obstacles. In noisy environments, where there are many small obstacles dispersed in the ultra sonic view range, the readings can give inaccurate and unstable information. Nevertheless, these sensors provide excellent sensing capabilities to implement obstacle avoidance algorithms.

The accelerometer represents a good input to determine the robot pose. The 8-bit resolution allows the reading of the roll and pitch angles with an average resolution of 1.5 $^{\circ}$. The I^2C communications were found to be reliable and fast enough for the amount of information exchanged.

The H-Bridges were a good solution, and although they have not been tested at the

full capacity, they allow the control of brushed electric motors with high loading currents.

The GPS module provided valuable information regarding the UAV position. The GPS signal reception was tested both in indoors and outdoors; in indoors the reception is only possible close to windows.

The two microcontrollers architecture proved its functionality. This design allowed the achievement of more processing capabilities and also retain the ability to introduce future improvements. The algorithm is running in two 16-bit MCU from the PIC24 family, which, together, provide together 40 I/O ports. The used sensors enabled a satisfactory sense of the vehicle pose and the surrounding environment.

Early flight tests are to be made in indoor environment, at LAR, to test the object detection system, and the low level control algorithms. This controlled environment will provide a good test site for the early flights tests. Simulating some of the common tasks, such as, take-off and landing, stabilization, position holding and remote controlled operation, will be possible to make conclusions regarding the overall system performance.

From these tests it is expected to validate, more specifically: the thrusters propulsion to adequately control the UAV, as determined in section 3.2.2; testing the UAV manoeuvrability; assess the robustness and the effectiveness in reducing the pitching moments of the structure solution implemented.

The flight experiments will enable to test the sensors effectiveness in a real scenario, since they were only been tested on the ground. The LAR represents a challenge to the UAV embedded control system since, the space available is considerably tight when compared to the vehicle dimension; in LAR there are also many sharp objects that can threaten the UAV integrity.

To allow a good mission management, and provide the desired situation awareness to the controller, the graphical interface effectiveness in the UAV control will be tested and improved from these tests.

6.1 Contributions of this thesis

With this thesis, a new research area, in the aerial robotics field, was started in LAR (Laboratório de Automação e Robótica). From the research and work developed in this thesis resulted a complete UAS. This UAS is composed by a LTA platform, its embedded control system and a ground station with an application to interface with the UAV.

Besides the fact that none of the solutions implemented is completely new, and that no remarkable breakthrough was achieved, the UAS as a whole has some novel solutions that were never implemented together before, achieving performances and capabilities not common on a low-cost lighter-than-air airship.

The implementation of ducted fans as vectoring thrusters allowed to improve the manoeuvrability of the UAV. The use of orientable camera and a ultrasonic range finder adds an extra value to the platform, providing a better sense of the surrounding environment. The use of sensors for object avoidance allows the implementation of an active security system, which can be used to fly the robot out of the operator line-of-sight. The custom-

designed control board provides a good starting point for future projects, allowing a wide range of sensors and actuators configuration.

The UAS developed constitutes a good platform for future research projects, due to its payload ability, robustness and reliability. Therefore, this project provides a contribution to the field of autonomous robotics airships.

6.2 Future Work

The cooperation among robots is an active search trend, and already proved its capabilities in a real scenario. After hurricane Wilma, an UAV and USV team accomplished together what a single UGV could not.This project can be used as a test bed for future developments and other research areas, namely cooperation among robots.

This platform offers a great tool, when paired with other UAV, to enable a higher covered area and multi-task assignments. But one of the biggest advantages is, perhaps, to use this platform to provide a bird-eye-view over the field, improving the integrated manoeuvrability of ground based robots.

The systems developed in this thesis are open to further research. The following topics would complement and improve the work developed in each of the UAS systems.

- On the high level control algorithm the following possibilities, are highlighted:
  - cooperative UGV;
  - integrate this platform in a swarm robotics approach;
  - develop the autonomy capabilities;
  - improve the image acquisition system and develop visual based algorithms.
- The GUI application could be complemented with:
  - the imagery information being embedded in the graphical interface;
  - use a joystick or keyboard as an input for the manual mode control;
  - improve the image acquiring system and develop visual algorithms.
- On the sensory level, the following improvements are proposed:
  - implement an additional GPS module in the ground station for differential GPS;
  - research and evaluate the improvements with other sensors;
  - test the board developed within other vehicles.

Appendix A

Telemetry messages description

Table A.1: Message fields, organized by their data type.

type	description	header	format	units
Sender	UAV identification key	BLIMP1		
	Ground station identification key	GROUND		
UAV pose	latitude	LAT	40.7835107	°
	longitude	LON	08.5597483	°
	altitude	ALT	12.00	m
	roll	ROL	10.0	°
	pitch	PIT	10.0	°
	yaw	YAW	62.0	°
	velocity	VEL	4.5	$m.s^{-1}$
Sensors	sonar	SOx	5.55	m
	accelerometer	ACx	1.0	G
	magnetometer	MGx	1.00	OE
	gyroscope	GYx	40.00	$°.s^{-1}$
Hardware	H-Bridge	HBx	40	%
	servo	SEx	40	°
	LED	LED	50	%
	PWM2	PMx	50	%
	auxiliary outputs	Axx[1]	40	bool
GPS solution info	date & time	DAT	010109.0830	ddmmyy.hhmm
	Horizontal DOP	HDO	1.5	dimensionless
	Vertical DOP	VDO	1.0	dimensionless
	Position DOP	PDO	2.0	dimensionless
	number of satellites	SAT	05	dimensionless
Additional info	emergency states	WAR	1	bool
	autonomous operation mode	MAN	0	bool
	wind speed	WNS	0.5	$m.s^{-1}$
	wind direction	WND	15	°
	way-point coordinates	WAx	lat,lon,alt	°, °, m
	thrusters regime	THR	100	%
	vectoring thrust angle	VTA	99	º
	tail thruster regime	TTR	00	%

References

[1] autopilot: Do it yourself uav, 2005. [online]. Available: http://autopilot.sourceforge.net/ [Accessed: May, 08 2009].

[2] Custom UAV, 2008. [online]. Available. http://www.uavdev.com/index.html [Accessed: Aug, 17 2009].

[3] The paparazzi project, 2009. [online]. Available: http://paparazzi.enac.fr/wiki/Main_Page [Accessed: May, 10 2009].

[4] I.H. Abbott and A.E. Von Doenhoff. *Theory of Wing Sections: Including a summary of airfoil data*. Courier Dover Publications, 1959.

[5] AeroViroment. Raven small unmanned aircraft system, aeroviroment 2009 [online]. Available: http://www.avinc.com/media_gallery/images/uas/ [Accessed: Set. 12, 2009].

[6] Chris Anderson. How to add vectoring thrusters to a blimp, may 2008. [online]. Available: http://diydrones.com/profiles/blog/show?id=705844:BlogPost:37162 [Accessed: Jun. 02, 2009].

[7] Chris Anderson and Jordi Muñoz. Diy drones 2009. [online]. Available: http://diydrones.com/ [Accessed: May, 8 2009].

[8] José Azinheira, Victoria Ferreira, Alexandra Moutinho, and et. al. Dirigível instrumentado para vigilância aérea - gallery, [online]. Available: http://paloma.isr.uc.pt/projects/diva/images/media/pictures/ [Accessed: Sept. 10, 2009].

[9] McCormick Barnes W. *Aerodynamics, Aeronautics, and Flight Mechanics*. Wiley, 2nd edition, September 1994.

[10] Johan Bijker and Willem Steyn. Kalman filter configurations for a low-cost loosely integrated inertial navigation system on an airship. *Control Engineering Practice*, 16(12):1509 – 1518, 2008.

[11] J. Borenstein, editor. *Where am I? – Systems and Methods for Mobile Robot Positioning*. University of Michigan, 1996.

[12] Butterworth-Hayes. Uavs – a vision of the future. Euro-UVS publication, Newsdesk Communications Ltd, 2003.

[13] Michael J. Caruso. Applications of magnetoresistive sensors in navigation systems. Technical report, Honeywell Inc., 1997.

[14] Michael J. Caruso, Tamara Bratland, and Robert Schneider Dr. Carl H. Smith. A new perspective on magnetic field sensing. Technical report, Honeywell Inc., Nonvolatile Electronics, Inc., 1998.

[15] M.J. Caruso. Applications of magnetic sensors for low cost compass systems. In *Position Location and Navigation Symposium*, pages 177–184, 2000.

[16] Ely Carneiro de Paiva, Josè Raul Azinheira, Josuè G. Ramos Jr., Alexandra Moutinho, and Samuel Siqueira Bueno. Project aurora: Infrastructure and flight control experiments for a robotic airship. *Journal of Field Robotics*, 2006.

[17] Digi International Inc., 11001 Bren Road East Minnetonka, MN 55343. *XBee®/XBee-PRO® ZB RF Modules*, Aug. 2009.

[18] Alberto Elfes, Samuel S. Bueno, Marcel Bergerman, Ely C. de Paiva, Josué G. Ramos, and José R. Azinheira. Robotic airships for exploration of planetary bodies with an atmosphere: Autonomy challenges. *Autonomous Robots*, 14(2):147–164, 03 2003.

[19] Alberto Elfes, Samuel S. Bueno, Marcel Bergerman, and Josué Jr. G. Ramos. Project aurora: Development of an autonomous unmanned remote monitoring robotic airship. *Journal of the Brazilian Computer Society*, April 1998.

[20] Freescale Semiconductor. *Technical Data 5.0 A H-Bridge with Load Current Feedback*, rev 12.0 edition, Fev. 2007. `www.freescale.com/support`.

[21] Xing P. Guô, editor. *Robotics Research Trends*, chapter 2, pages 77–120. Nova Science Pub Inc, Jul. 30, 2008.

[22] Mike Hirst. *Airborne early warning: design, development, and operations*. Osprey, 1983.

[23] Smith Hubert C. *The illustrated guide to aerodynamics*. McGraw-Hill, 2nd edition, December 1, 1991.

[24] jarontec. uavplayground - an approach to unmanned aerial vehicles (uav) with java and the processing development environment, 2009 [online]. Available: `http://code.google.com/p/uavplayground/` [Accessed: Jun. 03, 2009].

[25] E. N. Johnson. *Springer Handbook of Robotics - Aerial robotics*. Springer Berlin Heidelberg, 2008.

[26] George Kantor, Sanjiv Singh, and David Wettergreen. Enviroblimp, carnegie mellon university - robotics institute, 2001. [online]. Available: `http://www.frc.ri.cmu.edu/projects/enviroblimp/` [Accessed: Out, 04 2009].

[27] J. Spencer King, Vito Sabella, Fu-Zu Jen, Scott Currie, and Chris Hoess. Stwing-seas blimp project, 2002. [online]. Available: `http://www.stwing.upenn.edu/blimp/index.shtml` [Accessed: Out, 04 2009].

[28] Peter Kungl, Markus Schlenker, Dirk-Alexander Wimmer, and Bernd Helmut Kroplin. Instrumentation of remote controlled airship "lotte" for in-flight measurements. *Aerospace Science and Technology*, 8(7):599 – 610, 2004.

[29] Simon Lacroix, Il-Kyun Jung, Philippe Soueres, Emmanuel Hygounenc, and Jean-Paul Berry. The autonomous blimp project of laas/cnrs – current status. *Experimental Robotics VIII*, pages 487–496, 2003.

[30] Edward Lewis, Houghton Peter, and William Carpenter. *Aerodynamics for engineering students*. Butterworth-Heinemann, 1st edition, March 2003.

[31] Long Maurice W., editor. *Airborne Early Warning System Concepts*. Artech House, 1992.

[32] Eugene Miasnikov. Terrorists develop unmanned aerial vehicles, December 2004. Center for Arms Control, Energy and Environmental Studies at MIPT.

[33] Eugene Miasnikov. Threat of terrorism using unmanned aerial vehicles: Technical aspects. Center for Arms Control, Energy and Environmental Studies at MIPT, June 2004. Available: `http://www.armscontrol.ru/UAV/report.htm` [Accessed: Aug. 13, 2009].

[34] Moran Michael J. and Shapiro Howard N. *Fundamentals of Engineering Thermodynamics*. Wiley, Jun. 11, 2003.

[35] MicroPilot. Micropilot: World leader in miniature uav autopilots, 2009. [online]. Available: `http://www.micropilot.com/` [Accessed: Nov. 11, 2009].

[36] Valerie Moolman. *The road to Kitty Hawk Epic of flight*. Time-Life Books, 1980.

[37] Robin R. Murphy and Daniele Nardi Satoshi Tadokoro et. al. *Springer Handbook of Robotics - Search and Rescue Robotics*. Springer Berlin Heidelberg, 2008.

[38] Office of Naval Research. Silver fox, office of naval research, 2003 [online]. Available: `http://www.onr.navy.mil/media/extra/fact_sheets/silver_fox.pdf` [Accessed: Sep. 12, 2009].

[39] Aníbal Ollero and Luís Merino. Control and perception techniques for aerial robotics. *Annual Reviews in Control*, 28(2):167 – 178, 2004.

[40] Tom Pycke. Mav-blog - stuff related to mav's (and uav's) from a hobbyist's point of view, 2009. [online]. Available: `http://tom.pycke.be/` [Accessed: Set, 13 2009].

[41] Robert Rizza. *Introduction to Mechanical Engineering*. Prentice Hall, Nov. 5, 2000.

[42] Alessandro Saffiotti. Platforms for rescue operations. Technical report, OrebroUniversity,Orebro,Sweden, 2003.

[43] Emanuel Stingu and Frank Lewis. A hardware platform for research in helicopter uav control. *Journal of Intelligent and Robotic Systems*, 54(1):387–406, 03 2009.

[44] Joshua Stoff. *Aviation Firsts: 336 Questions and Answers*. Courier Dover Publications, 2000.

[45] John Stowers. Albatross - the kiwi uav, 2007. [online]. `http://www.albatross-uav.org/index.php/Main_Page` [Accessed: Set, 14 2009].

[46] Horizon Fuel Cell Technologies. Aeropack: Experimental flight history, horizon 2009. [online]. Available: `http://www.horizonfuelcell.com/aerospace_history.htm` [Accessed: Aug. 18, 2009].

[47] Technology Corporation, 16, No.186,Chien 1 Road, 235Chung Ho City,Taipei Hsien, Taiwan ,R.O.C. *Product User Manual : EM-406A*, Aug. 2007.